



LUND UNIVERSITY

Nonlinear Frequency Control of an Ultrasonic Generator

Part II

Rosenberg, Michael

1995

Document Version:

Publisher's PDF, also known as Version of record

[Link to publication](#)

Citation for published version (APA):

Rosenberg, M. (1995). *Nonlinear Frequency Control of an Ultrasonic Generator: Part II*. (Technical Reports TFRT-7538). Department of Automatic Control, Lund Institute of Technology (LTH).

Total number of authors:

1

General rights

Unless other specific re-use rights are stated the following general rights apply:

Copyright and moral rights for the publications made accessible in the public portal are retained by the authors and/or other copyright owners and it is a condition of accessing publications that users recognise and abide by the legal requirements associated with these rights.

- Users may download and print one copy of any publication from the public portal for the purpose of private study or research.
- You may not further distribute the material or use it for any profit-making activity or commercial gain
- You may freely distribute the URL identifying the publication in the public portal

Read more about Creative commons licenses: <https://creativecommons.org/licenses/>

Take down policy

If you believe that this document breaches copyright please contact us providing details, and we will remove access to the work immediately and investigate your claim.

LUND UNIVERSITY

PO Box 117
221 00 Lund
+46 46-222 00 00

ISSN 0280-5316
ISRN: LUTFD2/TFRT--7538--SE

Nonlinear Frequency Control of an Ultrasonic Generator: Part II

Michael Rosenberg

Department of Automatic Control
Lund Institute of Technology
September 1995

Department of Automatic Control Lund Institute of Technology P.O. Box 118 S-221 00 Lund Sweden		<i>Document name</i> Internal Report	
		<i>Date of issue</i> September 1995	
		<i>Document Number</i> ISRN LUTFD2/TFRT--7538--SE	
<i>Author(s)</i> Michael Rosenberg		<i>Supervisor</i> Ulf Jönsson, Anders Rantzer	
		<i>Sponsoring organisation</i>	
<i>Title and subtitle</i> Nonlinear Frequency Control of an Ultrasonic Generator: Part II			
<i>Abstract</i> <p>The ultrasonic equipment used to seal packages consists of an electric generator which delivers energy to an ultrasonic stack. There is a need to use a control system to control the frequency of the generator, since the resonance frequency of the stack is time varying.</p> <p>In this report an approximate analysis method is derived, which simplifies the mathematical analysis of the ultrasonic system. This method is then used to examine the existing solution to the frequency control problem, and some major problems with this solution are presented.</p> <p>Next a new solution to the frequency control problem is presented, which uses the amplitude of the converter as feedback via a PLL. The new setup also gives an opportunity to keep the generator and stack matched during the whole sealing cycle. This new solution is superior to the existing solution, and simulations on a computer are made to validate to theoretical results derived. This report contains additional material compared to ISRN LUTFD2/TFRT-5522-SE</p>			
<i>Key words</i>			
<i>Classification system and/or index terms (if any)</i>			
<i>Supplementary bibliographical information</i>			
<i>ISSN and key title</i> 0280-5316			<i>ISBN</i>
<i>Language</i> English	<i>Number of pages</i> 57	<i>Recipient's notes</i>	
<i>Security classification</i>			

The report may be ordered from the Department of Automatic Control or borrowed through the University Library 2, Box 1010, S-221 03 Lund, Sweden, Fax +46 46 110019, Telex: 33248 lubbis lund.

Preface

This thesis fulfills the requirements for the Master of Science degree in Computer Science and Technology at Lund Institute of Technology, Sweden. The work was carried out during the fall of 1994 at AB Tetra Pak Research and Development and at the Department of Automatic Control. Since the thesis is mainly theoretical, I spent most of the time making calculations and simulations on a computer. The programs I used were MATLAB, Maple and OmSim. Some practical work was also carried out at AB Tetra Pak Research and Development.

Although this thesis is theoretical, it deals with a practical problem. Unfortunately there were no time to implement the solution presented in this thesis. It would, however, be interesting to see the results of such implementation in the future.

I would like to thank the following persons who have helped me during the work with this thesis: My supervisors at the Department of Automatic Control, Ulf Jönsson and Anders Rantzer and my supervisor Gert Holmström at Tetra Pak Research and Development. A special thank to the people who read this report and corrected the many errors. None mentioned, none forgotten. **Notice:** This report contains additional theory about the matching of the generator and stack, compared to the report ISRN LUTFD2/TFRT-5522-SS.

Michael Rosenberg

Lund, January 1995

Contents

Preface	iii
1. Principles of the Ultrasonic Heating Process	1
The Ultrasonic Sealing Unit	1
Why Frequency Control of the Generator ?	1
2. Modeling of the Ultrasonic Sealing Unit	3
Linear Admittance Model of the Ultrasonic Sealing Unit	3
State Space Description of the Ultrasonic Sealing Unit	5
The Stationary Behavior of the Admittance Model	6
Linear Amplitude Model of the Ultrasonic Sealing Unit	8
Summary	9
3. Model Validation	10
Model Validation of the Admittance Model	10
Transfer Function Estimation	10
Data Acquisition System	11
Model Validation of the Amplitude Model	12
Summary	12
4. Real Time Identification	13
Continuous Time Recursive Least Square Identification	13
Implementation of the Regression Filter	14
Excitation of the Input Signal	15
Drawbacks of the Continuous Time RLS Estimator	15
Comments on the Discrete Time RLS Estimator	16
Summary	16
5. The Phase-locked Loop	17
Definitions	17
Description of the Phase-locked Loop	17
Linear Model of the Phase-locked Loop	18
Description of the Loop Filter	20
Description of the Phase Detector	21
Summary	23
6. Model Simplification	24
Phase Signal Domain Stationary Behavior	24
Approximation of the Phase Signal Domain Dynamics	25
Summary	25
7. Using the PLL with the Admittance Model	26
Setup of the PLL with the Admittance Model	26
Transformation of the PLL/Admittance Model Setup	26
Selection of the Loop Filter	27
Approximation of the PLL/Admittance Model Setup	27
Problems with the PLL/Admittance Model Setup	28
Summary	30
8. Using the PLL with the Amplitude Model	31
Setup of the PLL with the Amplitude Model	31

Properties of the Amplitude Model	32
Transformation of the PLL/Amplitude Model Setup	32
Adaptation of the Coil L_0	33
Transformation of the L_0 Adjustment Setup	34
Investigation of Equilibrium Points	34
Linearization of the PLL/Adaptive Amplitude Model Setup	36
Design of the L_0 Adjustment Controller	39
Summary	42
9. Simulations	44
Simulation of the PLL/Amplitude Setup with L_0 Adjustment	44
Simulation of the Simplified System	46
Summary	47
10. Concluding Discussion	48
Summary	48
Conclusions	48
References	50
A. OmSim programs	I

1. Principles of the Ultrasonic Heating Process

Vibrations with frequencies from 20 kHz up to approximately 100 MHz are called *ultrasound*. These vibrations can be used in various applications and especially, as in the case of AB Tetra Pak, to weld plastic materials together to form a package. Ultrasonic heating is one of the sealing methods in current use, which all exhibit the same fundamental principle; both heat and pressure are applied to the packaging material. The plastic layers on the inside of the packaging material melts and the heat is removed. The material, still under pressure, is cooled off and finally the pressure is removed. The result is two layers of packaging material welded together.

The main principle of ultrasonic heating is to convert electrical energy into mechanical energy, which is then transferred into the packaging material and converted to heat. For more information about applications of ultrasound and details of ultrasonic welding, see [6].

The Ultrasonic Sealing Unit

The existing equipment is presented in Figure 1, and it consists of five parts: **the electric generator** which supplies electrical energy to the system. From the generator's point of view the whole system acts like an electrical load, which varies with time.

the converter for transferring the electrical energy into mechanical energy. The converter consists of piezo electric crystals.

the booster which amplifies the amplitude of the mechanical vibrations from the converter. The amplification gain is determined by the ratio of the masses of the upper and lower halves of the booster.

the sonotrode delivers the mechanical vibrations into the packaging material. The sonotrode also amplifies the vibrations, just like the booster.

the anvil is used to clamp the packaging material between itself and the sonotrode.

When the converter, booster and sonotrode are put together they are referred to as the *stack*. The stack is vibrating longitudinally and from the vibrations frictional heat is generated in the packaging material, which is placed between the sonotrode and the anvil. In order to get a sealing, the pressure between the sonotrode and the anvil must be high.

For more details on the different parts used to build the ultrasonic sealing unit, see [5] and [6].

Why Frequency Control of the Generator ?

The ultrasonic stack is a resonant system, i.e. there is one frequency (the *resonance frequency*) at which the stack is willing to oscillate. But the resonance frequency of the stack varies with time.

The reasons for the variation in resonance frequency are many. Different stacks have different resonance frequencies and different packaging materials gives different resonance frequencies. This motivates the use of a control system

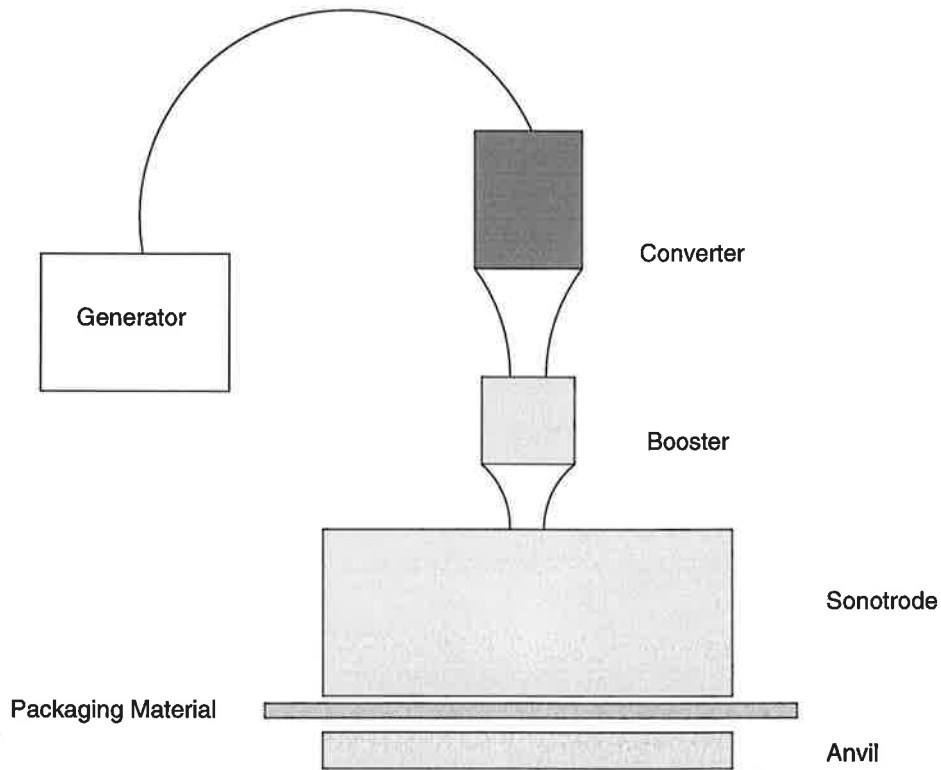


Figure 1. The ultrasonic sealing unit.

to make sure that the generator operates at the resonance frequency of the stack, which gives the most effective energy transport from the generator to the stack. The control system thus makes it possible to use the same generator for different stacks and different packaging materials, although their resonance frequencies differ.

Another reason for using frequency control is that during the sealing cycle the resonance frequency is changed due to compression in the package material and melting plastics. Practical experience also shows that the resonance frequency is dependent of the amplitude of the oscillations in the stack.

2. Modeling of the Ultrasonic Sealing Unit

There is a previous Master's thesis [5] which deals with the modeling of the ultrasonic sealing unit. In that work a description of how to use electrical analogies to describe mechanical systems is presented. Two different approaches to electrical modeling of mechanical systems are compared, the *lumped model* and the *transmission line model*, where the first is described by ordinary differential equations and the latter by partial differential equations. In the lumped model all information about the system is collected in a few parameters and no direct relation between these parameters and reality exists. This gives a fairly simple mathematical model of the system. The transmission line model relates each physical part of the system to a mathematical submodel, which makes it easy to understand the connection between reality and the model. Putting all submodels together gives a model of the total system, which is more complex than the lumped model.

Linear Admittance Model of the Ultrasonic Sealing Unit

In order to derive a mathematical model of the ultrasonic system some assumptions have to be made. First, the system is assumed to be *linear*, which is never true exactly. Next, the system is assumed to be *time invariant*, i.e. none of the parameters vary with time. This is really not true either. In practice the system depends strongly on time. With these limitations in mind, a linear time invariant model of the system can be derived.

A comparison between the transmission line model and the lumped model in the frequency domain showed great similarities in the interesting frequency range, so the lumped model probably contains enough information of the system. This fact, combined with the simpler mathematical structure of the lumped model, motivates the use of the lumped model in this thesis.

A commonly used (lumped) model to describe piezo electrical crystals is presented in Figure 2(a). Since the converter consists of piezo electrical crystals, this electrical equivalent circuit can be used to describe the converter. When the booster and sonotrode are connected to the converter, a new set of R , L , C and C_0 parameters is obtained¹. The mathematical structure of the model does not change. This means that the model only describes the behavior of the converter, but the model takes the *influence* of the booster and sonotrode on the converter into consideration.

The admittance of the circuit in Figure 2(a) is given by

$$Y(s) = \frac{I(s)}{U_1(s)} = sC_0 + \frac{1}{\frac{1}{sC} + R + sL} = \frac{C_0s(s^2 + \frac{R}{L}s + \frac{C_0+C}{LCC_0})}{s^2 + \frac{R}{L}s + \frac{1}{LC}}$$

When the generator and the stack are connected, there is a need to match the two systems to each other. This is done by connecting a coil L_0 between the generator and the stack (see Figure 2(b)), and the admittance seen from

¹ Table 5.1, page 31, in [5] justifies this statement.

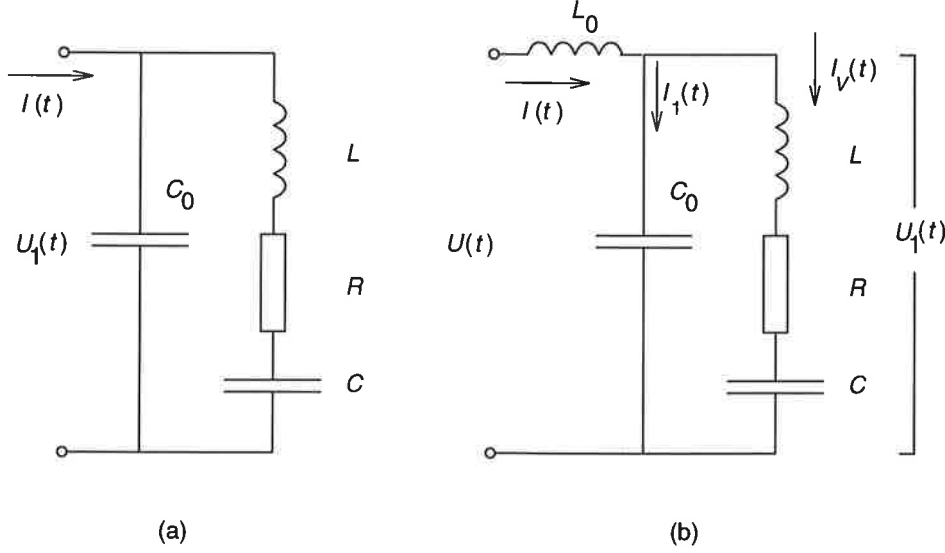


Figure 2. (a) Model of the stack. (b) Model of the total system.

the generator becomes

$$H_{UI}(s) = \frac{I(s)}{U(s)} = \left(sL_0 + \frac{1}{sC_0 + \frac{1}{\frac{1}{sC} + R + sL}} \right)^{-1} \quad (1)$$

This expression, which will be referred to as the *admittance model* or the *system*, can be rewritten after simple but tedious calculations as

$$H_{UI}(s) = \left(sL_0 + \frac{1}{sC_0} + \frac{-\frac{1}{C_0L}}{s^2 + \frac{R}{L}s + \frac{C_0+C}{LCC_0}} \frac{1}{sC_0} \right)^{-1} \quad (2)$$

The generator and the stack can only be matched at one frequency, so the *resonance frequency* is chosen. The resonance frequency is defined by

$$\omega_0 = \sqrt{\frac{C_0 + C}{LCC_0}} \quad (3)$$

and the booster and sonotrode, both mechanical resonators, are designed to have this resonance frequency. From now on it is assumed that *if the system in Figure 2(b) is working at the resonance frequency, the booster and sonotrode will also work at the resonance frequency*².

The generator and stack will be matched when $\arg\{H_{UI}(j\omega_0)\} = 0$. An examination of (2) shows that the argument of the last part of the expression equals zero at the resonance frequency. Using the $j\omega$ -method on the remaining part of the expression gives a constraint to decide L_0 at the resonance frequency, that is

$$\arg\{H_{UI}(j\omega_0)\} = 0 \quad \Leftrightarrow \quad j \left(\omega_0 L_0 - \frac{1}{\omega_0 C_0} \right) = 0$$

² This is an important statement, which will be used later when frequency control strategies are discussed.

which gives

$$L_0 = \frac{CL}{C_0 + C} \quad (4)$$

With this choice of L_0 the admittance seen from the generator will be real valued at the resonance frequency. This means that the phase shift between current and voltage will be zero, and all energy delivered by the generator will be consumed by the system. For other frequencies the load will become complex valued and energy will be returned to the generator. It is therefore of great importance that the generator is working close to the system's resonance frequency, and that the generator and stack are well matched.

An important interpretation of the model in Figure 2(b) is that the current $I_V(t)$ is the electrical analogy of the velocity of the converter, see [5]. Observe that this current is not measurable, since it does not exist in the real system. It is however possible to measure its mechanical analogy, the velocity. The only signals in Figure 2(b) with electrical correspondence are $U(t)$, $I(t)$ and $U_1(t)$. All other signals in the figure lack electrical correspondence in the real system, and have to be replaced by mechanical analogies.

Left to model is the generator, which has to ramp up the output voltage to avoid high transient currents during the start up process. This is very intuitive since the system needs a lot of energy in order to start to oscillate, thus forcing the generator to deliver a high current. When the system has started to oscillate, the amplitude of the output voltage from the generator is held constant.

In the derived model (1) there are four, in practice, time varying parameters. The electrical part of the converter C_0 is temperature dependent, but it varies only slowly with time and can be assumed to be constant during one sealing cycle. The variation is estimated to be $\pm 10\%$. Next the R parameter is highly dependent on the pressure in the system, which needs to be high to get good sealings. Finally the C and L parameters have no intuitive interpretation but they can be assumed to vary during a sealing cycle, although the variation is small.

State Space Description of the Ultrasonic Sealing Unit

Assuming that the parameters in the model of the total system (Figure 2(b)) do not vary with time, a state space model of the system can be derived. Using the signals introduced in the figure, the circuit is described by the following equations in the time domain

$$\begin{cases} U(t) &= L_0 \frac{dI}{dt} + U_1(t) \\ I(t) &= I_1(t) + I_V(t) \\ I_1(t) &= C_0 \frac{dU_1}{dt} \\ U_1(t) &= L \frac{dI_V}{dt} + RI_V(t) + \frac{1}{C} \int_0^t I_V(\tau) d\tau \end{cases} \quad (5)$$

Introducing the states

$$\begin{cases} \mathbf{x}_1(t) &= \int_0^t I_V(\tau) d\tau \\ \mathbf{x}_2(t) &= I_V(t) \\ \mathbf{x}_3(t) &= I(t) \\ \mathbf{x}_4(t) &= U_1(t) \end{cases}$$

gives $\dot{x}_1 = x_2(t)$ and $I_1(t) = x_3(t) - x_2(t)$. With these states (5) can be rewritten as

$$\begin{cases} \dot{x}_1 &= x_2(t) \\ U(t) &= L_0 \dot{x}_3 + x_4(t) \\ x_3(t) - x_2(t) &= C_0 \dot{x}_4 \\ x_4(t) &= L \dot{x}_2 + R x_2(t) + \frac{1}{C} x_1(t) \end{cases}$$

or in a more compact form

$$\dot{\mathbf{x}} = \begin{bmatrix} 0 & 1 & 0 & 0 \\ -\frac{1}{LC} & -\frac{R}{L} & 0 & \frac{1}{L} \\ 0 & 0 & 0 & -\frac{1}{L_0} \\ 0 & -\frac{1}{C_0} & \frac{1}{C_0} & 0 \end{bmatrix} \mathbf{x}(t) + \begin{bmatrix} 0 \\ 0 \\ \frac{1}{L_0} \\ 0 \end{bmatrix} U(t) \quad (6)$$

$$\begin{bmatrix} I(t) \\ I_V(t) \end{bmatrix} = \begin{bmatrix} 0 & 0 & 1 & 0 \\ 0 & 1 & 0 & 0 \end{bmatrix} \mathbf{x}(t)$$

where $\mathbf{x}(t) = [x_1(t) \ x_2(t) \ x_3(t) \ x_4(t)]^T$. This state space description of the ultrasonic system will later be used in the simulations.

The Stationary Behavior of the Admittance Model

Since the input to the system is a sinusoid, the equivalent circuit of the system can be analyzed with the $j\omega$ -method. It is important to be aware of the method's limitations. The $j\omega$ -method can only be applied to linear time invariant systems and it only gives information of the system's stationary behavior. No information of the system's transient behavior is given.

With these limitations in mind, it is seen that the admittance model (1) is indeed linear and assuming that the parameters only varies slowly with time, the system is approximately time invariant. Thus the $j\omega$ -method will give a good approximation of the system's stationary behavior.

Applying the $j\omega$ -method on the system (2) gives

$$\begin{aligned} H_{UI}(j\omega) &= \left(j \left(\omega L_0 - \frac{1}{\omega C_0} \right) - \frac{\frac{1}{C_0^2 L}}{-\frac{R}{L} \omega^2 + j\omega(\omega_0^2 - \omega^2)} \right)^{-1} \\ &= \left(\frac{R}{L^2 C_0^2 N(\omega)} + j \left(\omega L_0 - \frac{1}{\omega C_0} + \frac{1}{LC_0^2 N(\omega)} \frac{\omega_0^2 - \omega^2}{\omega} \right) \right)^{-1} \end{aligned}$$

where $N(\omega) = \left(\frac{R}{L}\omega\right)^2 + (\omega_0^2 - \omega^2)^2$. The amplitude and phase function for the system is now directly given by

$$A_{UI}(\omega) = \left(\left(\frac{R}{L^2 C_0^2 N(\omega)} \right)^2 + \left(\omega L_0 - \frac{1}{\omega C_0} + \frac{1}{LC_0^2 N(\omega)} \frac{\omega_0^2 - \omega^2}{\omega} \right)^2 \right)^{-\frac{1}{2}} \quad (7)$$

$$\varphi_{UI}(\omega) = -\arctan \left(\frac{L \omega_0^2 - \omega^2}{R \omega} + \frac{C_0^2 L^2}{R} N(\omega) \left(\omega L_0 - \frac{1}{\omega C_0} \right) \right)$$

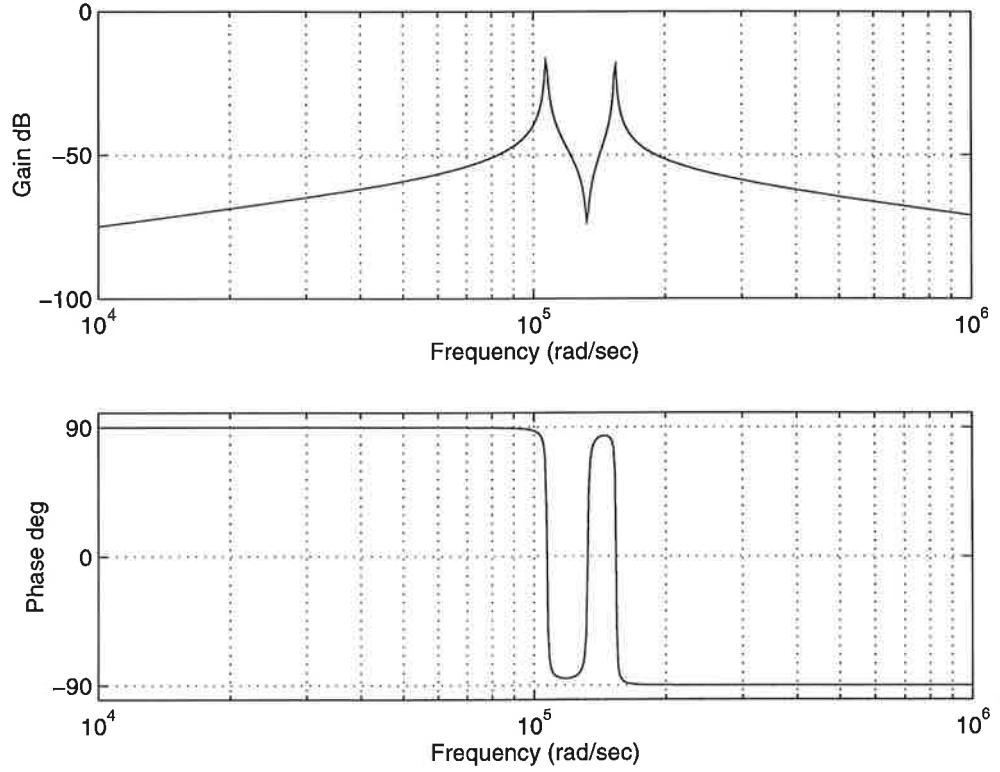


Figure 3. Bode plot of the admittance model $H_{UI}(s)$. Parameter values used: $C_0 = 15.8$ nF, $C = 2.18$ nF, $R = 50$ Ω , $L = 29.7$ mH and $L_0 = 3.60$ mH.

In stationarity, when the transients have disappeared, the output from the system is given by

$$I_{st}(t) = A_{UI}(\omega)U_0 \sin(\omega t + \varphi_{UI}(\omega))$$

where U_0 is the amplitude of the output voltage from the generator.

Assuming that the generator and stack are perfectly matched and that the generator is working at the resonance frequency ω_0 , the expression (7) for the amplitude and phase functions are simplified to

$$A_{UI}(\omega_0) = \frac{(C_0 + C)RC_0}{CL}$$

$$\varphi_{UI}(\omega_0) = 0$$

This gives the following expression for the output of the system when the perfectly matched system works in stationarity *and* at its resonance frequency

$$I_{st_0}(t) = \frac{(C_0 + C)RC_0}{CL}U_0 \sin \omega_0 t$$

In Figure 3 the amplitude and phase function for the admittance model (1) is plotted.

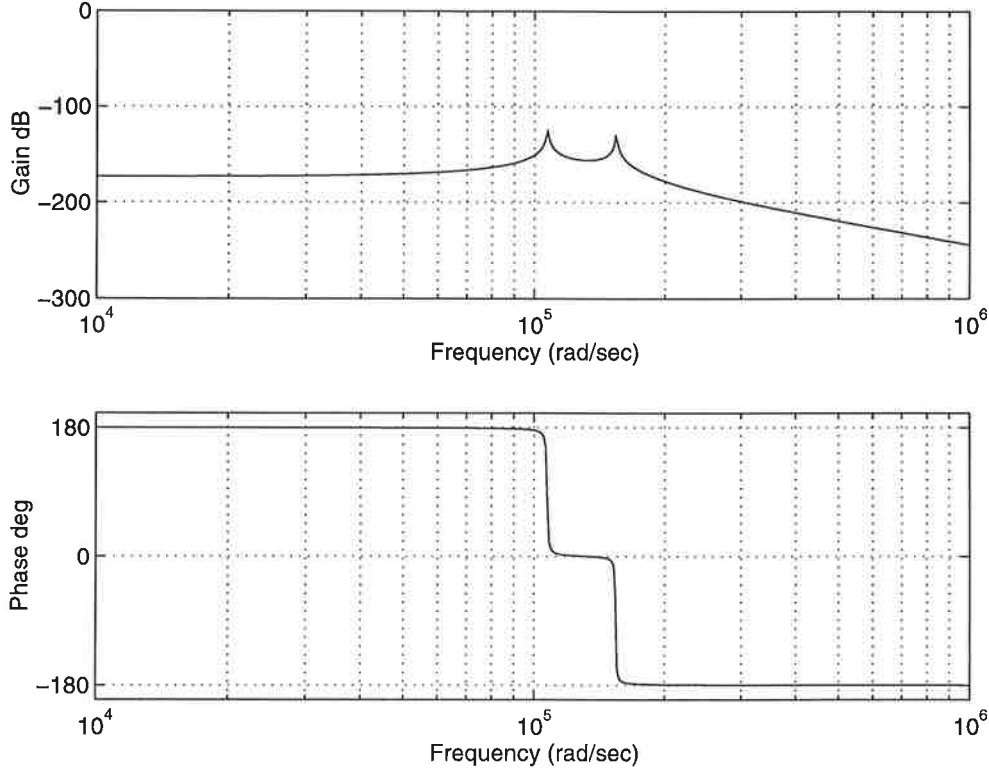


Figure 4. Bode plot of $-H_{UA}(s)$. Parameter values used: $C_0 = 15.8$ nF, $C = 2.18$ nF, $R = 50$ Ω , $L = 29.7$ mH and $L_0 = 3.60$ mH.

Linear Amplitude Model of the Ultrasonic Sealing Unit

An interesting relationship is the one between the output voltage from the generator and the amplitude of the stack. The model derived earlier used currents as electrical analogies for velocities. The current $I_V(t)$ in Figure 2(b) represents the velocity of the converter. The amplitude of the converter can easily be calculated as the integral of this velocity. Observe that this amplitude is *not* the same as the amplitude of the sonotrode. Both the booster and the sonotrode have a mechanical impedance and will both affect the amplitude. See [5] for a mechanical model of the booster and sonotrode. The same paper also contains a description on how to use electrical analogies.

Direct use of (5) gives the transfer function from $U(t)$ to $I_V(t)$. Integrating this expression, i.e. multiplying with $1/s$ in the frequency domain and introducing $I_A(t) = \int_0^t I_V(\tau)d\tau$, gives the transfer function from the voltage to the electrical analogy of the amplitude of the converter

$$H_{UA}(s) = \frac{I_A(s)}{U(s)} = \frac{\frac{1}{C_0 L L_0}}{s^4 + \frac{R}{L}s^3 + \left(\frac{1}{LC} + \frac{L_0+L}{C_0 L L_0}\right)s^2 + \frac{R}{C_0 L L_0}s + \frac{1}{C C_0 L L_0}} \quad (8)$$

This model will be referred to as the *amplitude model*.

Using the $j\omega$ -method and solving for the frequency when the imaginary part of $H_{UA}(j\omega)$ equals zero gives

$$\omega = \frac{1}{\sqrt{L_0 C_0}}$$

which is recognized as the resonance frequency ω_0 if the generator and stack are perfectly matched. At this frequency $H_{UA}(s)$ is independent of R . The phase shift between the output voltage from the generator and the amplitude of the converter is therefore independent of R and equals $-\pi$ radians. For convenience the sign of $H_{UA}(s)$ is changed, so the phase shift will become zero at the resonance frequency. Simple $j\omega$ -calculations gives the phase function of $-H_{UA}(s)$

$$\varphi_{UA}(\omega) = -\arctan\left(\frac{R}{L} \frac{\omega\left(\frac{1}{C_0 L_0} - \omega^2\right)}{\omega^4 - \left(\frac{1}{LC} + \frac{L_0+L}{C_0 L L_0}\right)\omega^2 + \frac{1}{C C_0 L L_0}}\right) \quad (9)$$

which is shown in Figure 4. Another important observation is that the slope of the phase function does not change sign for any R , which is the case with the phase curve of the admittance model.

Notice that the state $x_1(t)$ in (6) is the electrical analogy of the amplitude of the converter.

Summary

In this section a linear time invariant model of the ultrasonic sealing system was derived. An equivalent state space form is given in (6). A resonance frequency was defined and it was shown how to choose the coil L_0 , in order to match the generator and stack at the resonance frequency. When the model was derived some assumptions had to be made, and it is important to be aware of the limitations of the model. The real system is not linear and it is not time invariant. Specially R varies with time, but also C_0 which is temperature dependent. It should be noticed that some of the results derived are valid only for linear time invariant systems in stationarity (for example the Bode plots), and they should be used with care. The linear time invariant model derived is however mathematically attractive, and it will be used to gain insight in the ultrasonic system's behavior.

Two different transfer functions were derived, the admittance model and the amplitude model. The admittance model describes the admittance seen from the generator, and the amplitude model describes the connection between the output voltage from the generator to the amplitude of the converter.

Common for both models is that they only give information about the behavior of the converter, although the influence of the booster and sonotrode on the converter is modeled in the parameters R , L , C and C_0 . This means that nothing can be said about the behavior of the booster and sonotrode from the derived models. An important statement was however made, and it said that if the system in Figure 2(b) is working at its resonance frequency, then the whole stack is working at its resonance frequency, since the booster and sonotrode were designed to have this resonance frequency.

3. Model Validation

Two different models of the ultrasonic sealing unit have been derived in Section 2. In order to justify the use of these models, measurements must be made to show that the models correspond well with the real system. Measuring the transfer function for each of the two models would give enough information to motivate the use of the models. These measurements requires some knowledge about *system identification*.

For all measurements made, the amplitude of the input signal is much lower than the ordinary amplitude of the voltage from the generator. There are two reasons for this. First the models derived in Section 2 are linear and by using a small amplitude of the input signal the real system will hopefully behave linearly. The other reason is that there are some problems with high voltages in the converter, which makes it difficult to make the measurements.

Model Validation of the Admittance Model

Since the admittance model is previously known, no validation of this model is made in this thesis. Instead measurements made in [5] with the **HP 4194A Impedance Analyzer** are used to validate the admittance model. The measurements were made on the stack, which corresponds to the equivalent circuit given by Figure 2(a), but the admittance model also contains a coil L_0 . It is, however, easily realized that if the equivalent circuit in Figure 2(a) agrees well with the stack, then the equivalent circuit in Figure 2(b) will agree well with the total system.

The analyzer measures the impedance as a function of frequency, and the admittance is then given by inverting the impedance amplitude function and changing the sign of the impedance phase function. The analyzer also offers five different equivalent circuits to which the collected data can be matched. One of these five models is the circuit presented in Figure 2(a) so an estimate of the parameters in that model can easily be obtained. The estimated model can then be compared with the collected data to see how well the model and the real system correspond.

The measurements in [5] shows that the equivalent circuit of the stack agrees well with the real system, which implies that the admittance model is valid, and there is no need to repeat the measurements here.

Transfer Function Estimation

Denoting the input signal to the system $u(t)$ and the output signal from the system $y(t)$ their discrete Fourier transforms are given by

$$\begin{aligned} Y(j\omega) &= \mathcal{F}\{y(kh)\} \\ U(j\omega) &= \mathcal{F}\{u(kh)\} \end{aligned}$$

A simple transfer function estimate is then given by

$$\hat{H}(j\omega) = \frac{Y(j\omega)}{U(j\omega)}$$

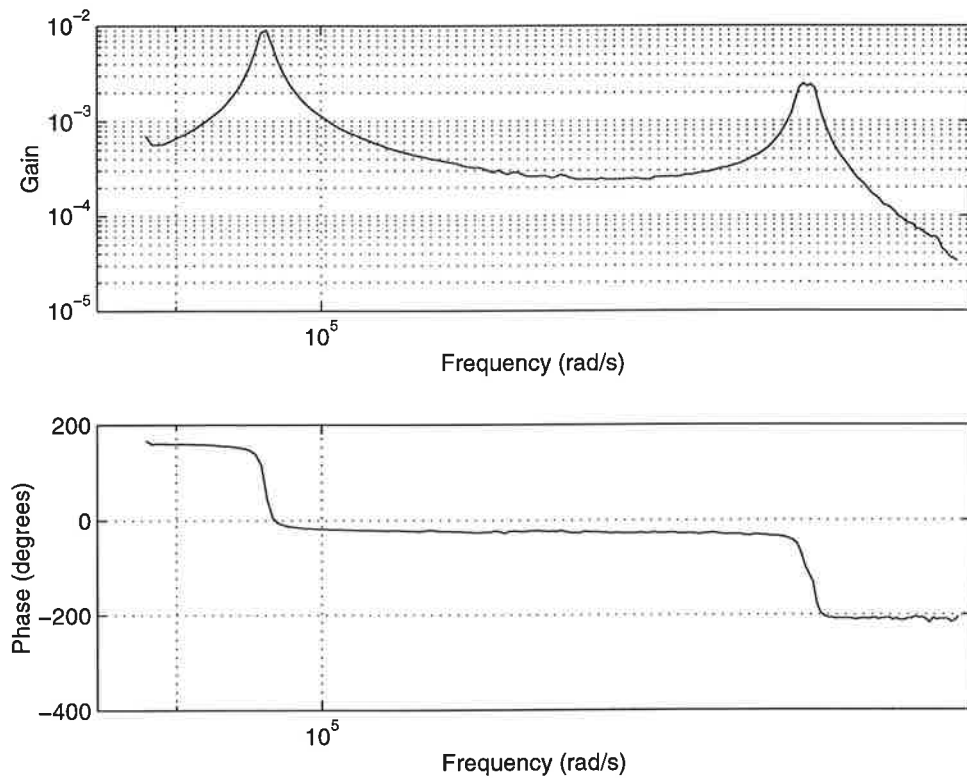


Figure 5. Measured Bode plot for the amplitude model.

which can be expected to give a good estimation of the continuous time system, if the signals $u(t)$ and $y(t)$ are sampled fast enough.

See Chapter 4 in [4] for more information on this system identification method.

Data Acquisition System

The interesting frequency range for the ultrasonic sealing system is approximately 15 kHz - 25 kHz, and the sampling frequency must be chosen fast enough to fulfill the sampling theorem. Since the generator output also contains higher order harmonics, consideration must be taken to implement anti aliasing filters.

The **HP 3567A** system takes care of these matters. It has an effective bandwidth up to 102.4 kHz and it also has the anti aliasing filters needed. Data can be collected from maximum six independent channels, and all measurements are stored in buffers. The information in these buffers can later be transferred to a computer and analyzed, either in a special **HP 3567A** program or exported to some other program. In the **HP 3567A** program there are possibilities to view the frequency contents of the collected data, power spectrum estimation and much more.

See [3] and Section 5.3.2 in [6] for a description of the program.

Model Validation of the Amplitude Model

To validate the transfer function (8) from the generator voltage to the amplitude of the converter, an amplitude measurement must be made. This was done with an optical amplitude sensor **MTI-1000 Fotonic Sensor**. Since the sensor is optical it is important that the measurements are made perpendicular to a surface that reflects the light. This surface can be found on the top of the converter, but this point does not correspond to the amplitude in the model. There is however a simple relation between the amplitude in the model and the measured amplitude. It can also be expected that the optical sensor will introduce an extra phase shift and amplitude distortion. In Section 5.3.1 in [6] the optical sensor is more detailed described.

The system under test (SUT) consisted of a variable coil and a converter. The coil were adjusted in order to match the converter. As the input signal to the SUT a *chirp signal* was used, i.e. a sinusoidal signal with a variable frequency. The frequency were swept from 15 kHz to 25 kHz with a sweep time of approximately 5 seconds, and it was generated by a **Leader LFG-1300 Frequency Generator**.

Both the chirp signal and the resulting amplitude signal were sampled by the **HP 3567A** and windowed by a Hanning window. The transfer function estimate was then calculated by the program. The resulting amplitude and phase function for the transfer function is shown in Figure 5, and the result shows great similarities between the model and the real system (compare Figure 4). This motivates the use of the amplitude model.

Summary

In this section measurements were made to justify the use of the models derived in Section 2. The validation of the admittance model were made by referring to measurements made in [5]. The amplitude model was however not previously known, and a validation of that model was done. The result shows that the amplitude model agrees well with the real system. This means that the use of both the admittance model and the amplitude model is justified.

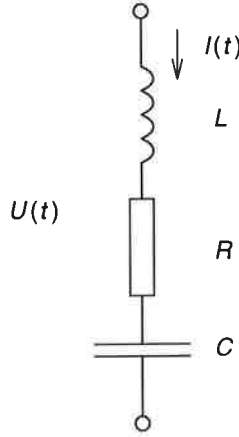


Figure 6. Second order resonant system.

4. Real Time Identification

Real time identification methods are algorithms used to identify a system in real time. The algorithms are usually recursive algorithms that updates the parameter estimates every time new data is collected. A problem with these methods is to get the parameter estimates to converge.

A real time recursive identification algorithm is an attractive concept to apply to the ultrasonic equipment, since the process typically contains parameters that vary with time. These parameters can be estimated in real time and the systems resonance frequency can be calculated. The frequency of the generator is then set to the estimated resonance frequency of the system.

Continuous Time Recursive Least Square Identification

For simplicity only the series resonance model in Figure 6 is considered. This is a continuous time model. Introducing the *damping* $\zeta = \frac{R}{2} \sqrt{\frac{C}{L}}$ and the *resonance frequency* $\omega_0 = \frac{1}{\sqrt{LC}}$, the admittance for the resonant system is given by

$$Y_1(s) = \frac{I(s)}{U(s)} = \frac{\frac{1}{L}s}{s^2 + \frac{R}{L}s + \frac{1}{LC}} = \frac{\frac{1}{L}s}{s^2 + 2\zeta\omega_0s + \omega_0^2} \quad (10)$$

In the time domain the expression can be written as

$$(p^2 + 2\zeta\omega_0p + \omega_0^2) I(t) = \frac{1}{L}pU(t)$$

where $p = \frac{d}{dt}$ is the differential operator. Reorganizing gives

$$p^2I(t) = -2\zeta\omega_0pI(t) - \omega_0^2I(t) + \frac{1}{L}pU(t) \quad (11)$$

This is an expression that includes derivatives up to order two. Therefore a *regression filter* $1/A(p)$ is introduced with $\deg A(p) \geq 3$, and the filter can be chosen as

$$\frac{1}{A(p)} = \frac{d^3}{(p+d)^3}$$

Multiplying both sides of (11) with the regression filter eliminates the problem with the derivatives and the expression turns into

$$I_f(t) = \frac{p^2}{A(p)}I(t) = -2\zeta\omega_0 \frac{p}{A(p)}I(t) - \omega_0^2 \frac{1}{A(p)}I(t) + \frac{1}{L} \frac{p}{A(p)}U(t) \quad (12)$$

Introducing vector notation gives

$$I_f(t) = \begin{bmatrix} -\frac{p}{A(p)}I(t) & -\frac{1}{A(p)}I(t) & \frac{p}{A(p)}U(t) \end{bmatrix} \begin{bmatrix} 2\zeta\omega_0 \\ \omega_0^2 \\ \frac{1}{L} \end{bmatrix} = \varphi^T(t)\theta$$

where $\varphi^T(t)$ is the *regression vector* and θ is the *parameter vector*. The *recursive least square* (RLS) estimator in continuous time is now given by (see [8], page 71)

$$\begin{cases} \frac{d\hat{\theta}}{dt} = P(t)\varphi(t) (I_f(t) - \varphi^T(t)\hat{\theta}(t)) \\ \frac{dP}{dt} = \alpha P(t) - P(t)\varphi(t)\varphi^T(t)P(t) \end{cases} \quad (13)$$

where α is the *forgetting factor* and $P(t)$ is the *covariance matrix*. This is a symmetric matrix, i.e. $P(t) = P^T(t)$. The forgetting factor α is used to make the RLS "forget" old data and to be able to track time varying parameters. More information on the RLS is given in [8], Chapter 3.

There are two ways to expand the RLS derived for the second order system to the ultrasonic system, given by the fourth order system in Figure 2(b). The first way is to expand the RLS derived above to include all four parameters in Figure 2(b). This would give a high order P -matrix, which implies that the implementation of the RLS may be complicated. With the parameter estimates obtained, it is then possible to estimate the resonance frequency of the system.

The second way is to assume that $I_V(t)$, which corresponds to the velocity of the converter, is measurable. The RLS already derived can then be used to estimate the R , L and C parameters. Measuring the generator current $I(t)$ makes it possible to calculate the current through the capacitance C_0 as $I(t) - I_V(t)$. The voltage $U_1(t)$ is measurable and thus an estimate of C_0 can easily be obtained. Now all parameters of the system are estimated, and an estimate of the resonance frequency is directly given by (3).

Implementation of the Regression Filter

In (12) it is seen that there is a need to filter four signals. This would normally require four filters but because of the problem's special structure, there is a way to design the regression filter which reduces the number of filters needed to two. Denote the output signal from the filter $Z(t)$, and the filter can be written

$$p^3\{Z(t)\} + 3dp^2\{Z(t)\} + 3d^2p\{Z(t)\} + d^3Z(t) = d^3I(t)$$

Introducing the states $x_1(t) = Z(t)$, $x_2(t) = p\{Z(t)\}$ and $x_3(t) = p^2\{Z(t)\}$ gives the following state space description

$$\begin{cases} \dot{x}_1 = x_2(t) \\ \dot{x}_2 = x_3(t) \\ \dot{x}_3 = -d^3x_1(t) - 3d^2x_2(t) - 3dx_3(t) + d^3I(t) \end{cases}$$

Denoting the components in the $\varphi(t)$ vector $\varphi_1(t)$, $\varphi_2(t)$ and $\varphi_3(t)$ it is easy seen that $\varphi_1(t) = -x_2(t)$, $\varphi_2(t) = -x_1(t)$ and $I_f(t) = x_3(t)$. Still there is a need for a second regression filter to filter $U(t)$ in order to get $\varphi_3(t)$.

Excitation of the Input Signal

In order to get convergence in the RLS the input signal to the system, i.e. the output signal from the generator, has to be of *sufficient excitation*. It is the excitation of the input signal that determines how many parameters in the model that can be estimated.

The signal acting in the ultrasonic system is mainly the sinusoid from the generator. A sinusoid signal is exciting of order 2, i.e. it is possible to determine only two parameters in the model. This is clearly a problem since there is a need to determine more parameters to estimate the resonance frequency. However, it can be observed that the frequency of the generator is varying (in its attempts to track the resonance frequency), which means that in practice the signal from the generator will be exciting of an order higher than 2. There will also be higher order harmonics acting on the system since the generator uses a square wave signal to produce the sinusoidal output signal.

It can also be observed that when the generator is started up, the voltage is ramped in some way in order to avoid high currents. Consider the case when the startup output voltage from the generator is given by

$$U(t) = t \sin \omega_0 t$$

The frequency contents of this signal is given by the Fourier transform

$$U(\omega) = \frac{j2\omega_0\omega}{(\omega_0^2 - \omega^2)^2}$$

which shows that the signal contains more frequencies than only ω_0 . This implies that there may be sufficient excitation to get estimates of the parameters needed to estimate the resonance frequency, at least under the startup process. However, this is not easy to analyze theoretically so it has to be tested in simulations.

Drawbacks of the Continuous Time RLS Estimator

There are some problems with the RLS estimator approach. The problem with the lack of excitation of the input signal will probably become worse when the RLS estimator is applied to the admittance model, since it is necessary to estimate four parameters. Also the alternative with the measurement of $I_V(t)$ can be expected to give problems due to lack of excitation, since three parameters needs to be estimated.

It may also be hard to implement the RLS in practice. There is a need to implement 14 first order differential equations using analog components, and a high number of multiplications.

Comments on the Discrete Time RLS Estimator

One way to get around the problem with the implemental issue of the continuous time RLS is to use a discrete time RLS. This can be implemented as formulas in a computer program, where the computer samples the $U(t)$ and $I(t)$ signals acting in the system. The discrete time RLS estimates the parameters in the model and calculates the resonance frequency of the system. The output frequency of the generator is chosen as the estimated resonance frequency. There are however some problems with this approach.

The first problem deals with the sampling of the process. In [7] expressions for the sampled system are derived when the input signal to a process is piecewise constant. This is the case when a first order hold D/A converter is used to control the input signal to the process. In this problem, the input signal is a sinusoid. Therefore none of the expressions derived in [7] can be used, since it is the input frequency that is piecewise constant. One way to get around this problem may be to use a first order hold circuit, which is a better approximation to a sinusoid than the zero order hold circuit. Another way is to recalculate the expressions in [7] for a sinusoidal input signal.

The next problem is that the discrete time RLS will probably need to sample the signals very fast. This, in combination with the calculations needed to calculate the estimates, implies that there will be high demands on the hardware used.

Another problem is when a continuous time system is sampled the resulting discrete time system often contains more parameters. This makes the problem with excitation worse, since more parameters has to be estimated.

There is also a problem with the estimation of the resonance frequency. This frequency can be calculated from the estimated discrete time parameters, but the relation between the resonance frequency and these parameters is complicated. Numerical problems may occur.

See [4] and [8] for a description of the discrete time recursive least square estimator.

Summary

In this section a continuous time recursive least square estimator was derived for a second order system. The estimator was used to estimate the parameters in a second order model, from which an estimate of the resonance frequency could be calculated.

The second order system was chosen for simplicity, and it was shown how the RLS could be expanded to estimate the four parameters in the total system.

Some problems with this approach to the frequency control problem was also discussed.

5. The Phase-locked Loop

The phase-locked loop (PLL) is an electrical device which can be used to synchronize two systems with sinusoidal signals to each other. More specifically this is done by changing the frequency of the PLL's internal oscillator in such a way that the phase difference between the input signal and the oscillator will approach zero, or at least remain small.

Definitions

In order to understand the PLL some definitions must be made. First the function $\theta(t)$ of a sinusoidal signal $\sin \theta(t)$ is called the *phase*. Then the *phase error* between two such signals is defined by

$$\theta_e(t) = \theta_1(t) - \theta_2(t)$$

Typically $\theta_1(t) = \omega_1 t + \varphi_1$ and $\theta_2(t) = \omega_2 t + \varphi_2$ which gives the phase error

$$\theta_e(t) = (\omega_1 - \omega_2)t + \varphi_1 - \varphi_2$$

where ω_1 and ω_2 are the *angular frequencies* of the signals. It is easily seen that this is a ramp function, but when both signals have the same angular frequency the phase error becomes constant.

There is a fundamental connection between the phase of a signal and the signal's angular frequency, defined by

$$\omega = \frac{d\theta}{dt} \quad (14)$$

From now on the angular frequency will be referred to as the frequency.

Description of the Phase-locked Loop

The main principle of the PLL is to keep the phase error between two signals small, one external $u_1(t)$ and one internal $u_2(t)$. This is done by changing the phase of the internal signal $u_2(t)$ of the PLL. This means that when the phase error in the PLL is small (the PLL is *locked*), the frequency of the internal signal is the same as the frequency of the external signal. At the same time the phase error between the two signals is zero, or at least very small. When the PLL has reached this locked state it is able to track changes in phase of the input signal. But if the rate of change in the phase of the external signal is too high, the PLL might *unlock* and once again it has to lock onto the external signal. It is of great importance to understand the mechanisms behind the PLL's behavior. A closer study of the PLL shows that there are four key parameters specifying the frequency range in which the PLL can be operated:

- The *lock range* $\Delta\omega_L$. This is the frequency range within which a PLL locks very quickly, and it is the normally operating frequency range.
- The *pull-in range* $\Delta\omega_P$. In this range the PLL will always become locked, but the process can be rather slow.

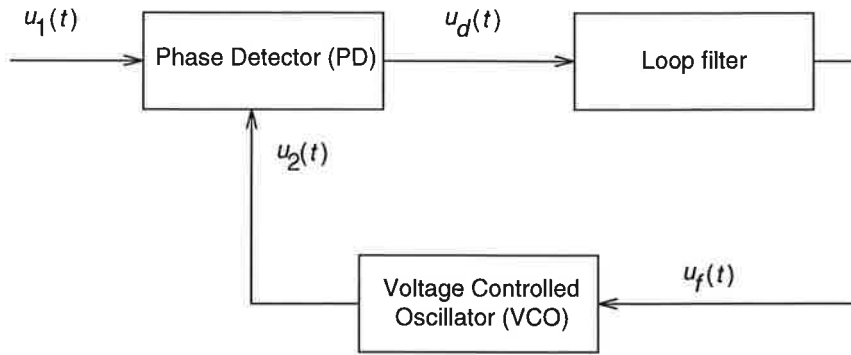


Figure 7. The three basic functional blocks of the PLL.

- The *hold range* $\Delta\omega_H$. This is the frequency range in which the PLL can statically maintain phase tracking.
- The *pull-out range* $\Delta\omega_{PO}$. If tracking is lost within this range a slow pull-in process is needed to lock the PLL again.

These parameters are discussed in detail in [1] Chapter 3 and [2] Chapter 5. Both authors also derive expressions for each parameter which can be used to estimate the size of each frequency range.

Physically the PLL consists of three basic functional blocks (see Figure 7):

- A phase detector (PD)
- A loop (low pass) filter
- A voltage-controlled oscillator (VCO)

In the PD the phase of the input signal $u_1(t)$ is compared against the phase of the signal $u_2(t)$ from the VCO and the PD gives an output $u_d(t)$ which depends on the phase error between the two signals, that is

$$u_d(t) = f(\theta_e)$$

The function $f(\cdot)$ depends on the type of PD used. Following the PD there is a low pass filter used to filter the signal from the PD, which often contains high frequencies. The choice of the filter is arbitrary, but usually a first order active or passive low pass filter is chosen. Finally the frequency of the output signal from the VCO is given by

$$\omega(t) = \omega_c + \Delta\omega(t)$$

where ω_c is the *center frequency* of the VCO and $\Delta\omega(t)$ is the *frequency deviation* from the center frequency. The frequency deviation is given by $\Delta\omega(t) = K_0 u_f(t)$ where K_0 is the VCO gain and $u_f(t)$ is the output of the loop filter.

Linear Model of the Phase-locked Loop

A mathematical treatment of the PLL is very complicated because of the nonlinear behavior of the PD, causing the differential equation that describes the PLL to become nonlinear. One way to simplify the problem is to assume

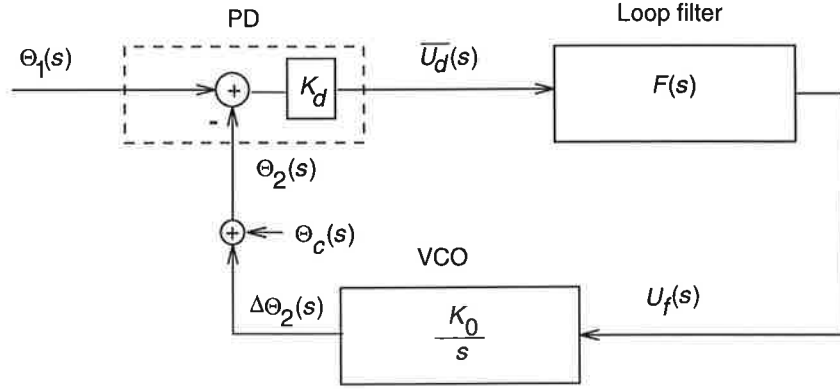


Figure 8. The linear model of the PLL in the locked state.

that the PLL is locked. This means that the phase error between $u_1(t)$ and $u_2(t)$ is small. The *average* output of the PD is assumed to be linear for small phase errors, which gives

$$\bar{u}_d(t) = K_d \theta_e(t) = K_d(\theta_1(t) - \theta_2(t)) \quad (15)$$

where K_d is the *phase detector gain*, $\theta_1(t)$ is the phase of the input signal and $\theta_2(t)$ is the phase of the signal from the VCO. In Figure 8 a block scheme of the linear PLL is shown. This approximation of the PD is true for a lot of different types of PD:s if the phase error is small.

The PLL has now been transformed from the *sinusoidal signal domain* into the *phase signal domain*, since all sinusoidal signals has been replaced with their corresponding phase signals. This is an important transformation which simplifies the analysis of the PLL.

Applying the Laplace transform to (15) gives the transfer function of the phase detector

$$\frac{\bar{U}_d(s)}{\Theta_e(s)} = K_d$$

Furthermore the differential equation describing the loop filter is assumed to be known and its transfer function is denoted $F(s)$. Left to be found is the transfer function of the VCO. Using the relation (14) on the expression for the frequency of the output signal from the VCO yields

$$\theta_2(t) = \int_0^t (\omega_c + K_0 u_f(\tau)) d\tau = \omega_c t + K_0 \int_0^t u_f(\tau) d\tau = \theta_c(t) + \Delta\theta_2(t)$$

where $\theta_c(t) = \omega_c t$ is the *center phase* and $\Delta\theta_2(t)$ is the *phase deviation* from the center phase. Since only the phase deviation is interesting, the contribution from the center phase is from now on neglected in the calculations. The transfer function of the VCO is then directly given by

$$\frac{\Delta\Theta_2(s)}{U_f(s)} = \frac{K_0}{s}$$

It is always possible to write the input phase signal on the form

$$\theta_1(t) = \theta_c(t) + \Delta\theta_1(t)$$

where $\theta_c(t)$ will disappear in the PD. It is now easy to calculate $\Theta_e(s)$ as a function of $\Delta\Theta_1(s)$

$$\Theta_e(s) = \frac{s}{s + K_0 K_d F(s)} \Delta\Theta_1(s)$$

This equation can be used to derive an expression for the steady state phase error for different $\theta_1(t)$. First a step change in the phase is considered, i.e.

$$\theta_1(t) = \omega_c t + \Delta\varphi \cdot u(t)$$

where $u(t)$ is the step function. Laplace transforming the deviation from the center phase gives

$$\Delta\Theta_1(s) = \frac{\Delta\varphi}{s}$$

and applying the final value theorem gives

$$\lim_{t \rightarrow \infty} \theta_e(t) = \lim_{s \rightarrow 0} s \Theta_e(s) = \lim_{s \rightarrow 0} s \frac{s}{s + K_0 K_d F(s)} \frac{\Delta\varphi}{s} = 0$$

Thus a step change in the input phase doesn't give rise to any steady state phase error. Now consider the case when a step change in frequency is applied to the input phase. This means that

$$\theta_1(t) = (\omega_c + \Delta\omega \cdot u(t))t = \omega_c t + \Delta\omega t \cdot u(t)$$

which gives the Laplace transform of the deviation from the center phase

$$\Delta\Theta_1(s) = \mathcal{L}\{\Delta\omega t \cdot u(t)\} = \frac{\Delta\omega}{s^2}$$

and the final value theorem gives

$$\lim_{t \rightarrow \infty} \theta_e(t) = \lim_{s \rightarrow 0} s \Theta_e(s) = \lim_{s \rightarrow 0} s \frac{s}{s + K_0 K_d F(s)} \frac{\Delta\omega}{s^2} = \frac{\Delta\omega}{K_0 K_d F(0)} \quad (16)$$

A step change in the frequency of the input phase signal thus produces a steady state phase error. Notice however that the error depends on the type of loop filter used, which will be discussed next.

Description of the Loop Filter

Four types of loop filters are presented in [1], Table 2.2 page 13. The simplest filter, called type 1, is a one pole low pass filter with the transfer function

$$F(s) = \frac{1}{1 + \tau s} \quad (17)$$

and $F(0) = 1$. The steady state phase error caused by a step change of the frequency of the input signal can now be calculated from (16), which yields

$$\lim_{t \rightarrow \infty} \theta_e(t) = \frac{\Delta\omega}{K_0 K_d F(0)} = \frac{\Delta\omega}{K_0 K_d}$$

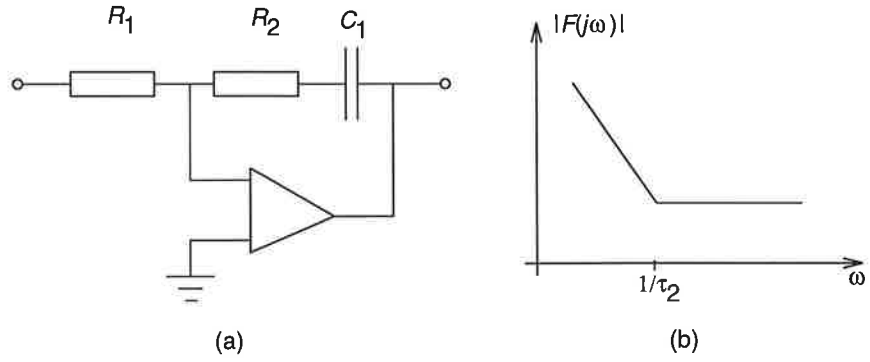


Figure 9. (a) An implementation of the active low pass filter. (b) Amplitude function for the active filter.

In practice K_0 is usually large so the steady state phase error will become small. Next an active filter, called type 3 or a *charge pump*, is considered. Its transfer function is given by

$$F(s) = \frac{1 + \tau_2 s}{\tau_1 s} \quad (18)$$

and $F(0) = \infty$. For this filter the steady state phase error of a frequency step becomes

$$\lim_{t \rightarrow \infty} \theta_e(t) = \frac{\Delta\omega}{K_0 K_d F(0)} = 0$$

An implementation of the type 3 filter is shown in Figure 9(a) together with a simplified amplitude function for the filter (Figure 9(b)). Notice that it is important that the bandwidth of the operational amplifier in the active filter is large enough to handle the proportional gain at higher frequencies ($\omega > 1/\tau_2$).

Description of the Phase Detector

Many different types of phase detectors exist, and in [1] Table 2.1 page 8, four of them are presented. The first one is the PD type 1, which is an analog multiplier. This PD can be analyzed to understand the basic principles of all PD:s.

Assuming that the two input signals to the PD are given by $u_1(t) = A_1 \sin(\omega_1 t + \varphi_1)$ and $u_2(t) = A_2 \cos(\omega_2 t + \varphi_2)$, then the PD produces the output

$$u_d(t) = u_1(t)u_2(t)$$

and trigonometrics gives

$$u_d(t) = K_d (\sin((\omega_1 - \omega_2)t + \varphi_1 - \varphi_2) + \sin((\omega_1 + \omega_2)t + \varphi_1 + \varphi_2))$$

where $K_d = \frac{A_1 A_2}{2}$ is the amplitude dependent gain of the PD. The amplitude dependence can be removed by taking the sign of the input signals to the PD, but this will introduce higher order harmonics. If $\omega_1 \approx \omega_2$ and if the sinusoid with the frequency $\omega_1 + \omega_2$ is filtered out by the loop filter, the average output from the PD is given by

$$\bar{u}_d(t) = K_d \sin(\varphi_1 - \varphi_2) = K_d \sin \theta_e \approx K_d \theta_e$$

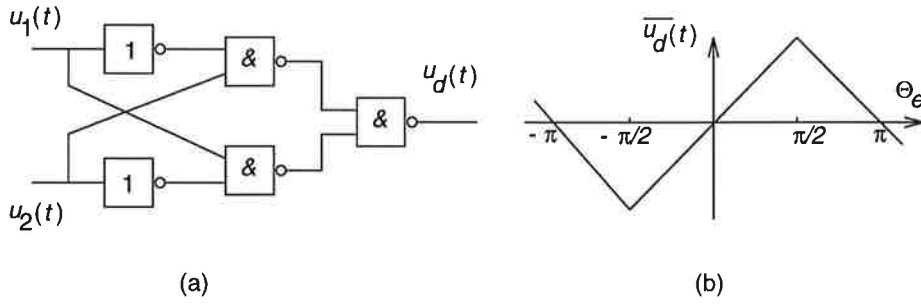


Figure 10. (a) An implementation of the type 2 phase detector. (b) Average output signal as a function of phase error for the PD type 2.

which is true if the phase error is small. This is the main principle of all PD:s. The PD produces a signal with the frequency difference and frequency sum of the two input signals. The sinusoid with the frequency $\omega_1 + \omega_2$ is filtered out by the loop filter and left is the term which is proportional to the phase error.

Other types of PD:s presented in [1] is the PD type 2 (also called the XOR-PD) and the PD type 4. Common for these both PD:s is that they are built from latches and that all signals working on the latches are square wave signals. These square wave signals can be obtained by taking the sign of the input signal $u_1(t)$ and the VCO signal $u_2(t)$. A PD build from these principles is called a *digital PD*, and both PD type 2 and PD type 4 are members of this category.

An implementation of the type 2 PD is shown in Figure 10(a) and by definition the phase error is zero when the phase shift between $u_1(t)$ and $u_2(t)$ is $\pi/2$. It is easily shown that the average output from this type of PD is given by

$$\bar{u}_d(t) = K_d \theta_e$$

in the range $-\pi/2 < \theta_e < \pi/2$ (see Figure 10(b)). Any type of loop filter can be used with this PD.

The type 4 PD is superior to type 2 PD in every regard except in simplicity. One special characteristic is that when the PLL isn't locked the PD type 4 produces an average signal that is approximately proportional to the frequency error, i.e

$$\bar{u}_d(t) \approx K'_d \omega_e$$

where K'_d is a new gain constant for the PD. Therefore the PD type 4 is also called a *frequency/phase detector*.

In the locked state the average output signal from the PD type 4 is given by

$$\bar{u}_d(t) = K_d \theta_e$$

which is valid in the range $-2\pi < \theta_e < 2\pi$. Notice, however, that $K_d \neq K'_d$. The frequency/phase detector is thus linear for a larger range of phase errors which justifies the linear approximation of the PLL made above. It is important to understand that the PLL's behavior is dependent on the type of PD used.

An alternative to the digital PD:s mentioned above is the *all digital PD*, which samples the input signal to the PLL and via software calculates the phase error.

Summary

In this section the basic theory for the phase-locked loop was presented. The three building blocks of a PLL are the phase detector, the loop filter and the voltage controlled oscillator. In order to analyze the PLL mathematically, some approximations had to be made. First the average output from the phase detector was assumed to be directly proportional to the phase error, and secondly the phase error was assumed to be small. Under these assumptions, the PLL could be transformed from the sinusoidal signal domain into the phase signal domain. This transformation simplified the analysis of the PLL.

Some different phase detectors were presented and the basic principle of these was shown. It was also shown that the loop filter should be an active low pass filter in order to avoid stationary phase errors.

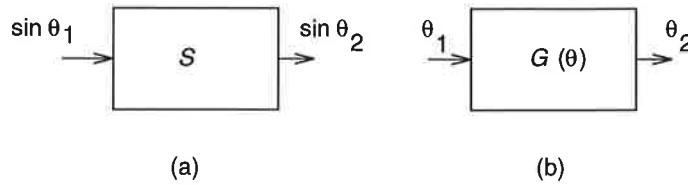


Figure 11. (a) Relations in the sinusoidal signal domain. (b) Relations in the phase signal domain.

6. Model Simplification

The admittance model and the amplitude model presented in Section 2 are complex. They both use a system of four first order differential equations to describe the reality. This means that it may be very time consuming to simulate the systems on a computer. It is therefore interesting to simplify the models previously derived. It would also be preferable to make a simplification that makes it possible to connect the PLL and the stack in the phase signal domain.

Phase Signal Domain Stationary Behavior

In Section 5 a linear model of the PLL was derived. The simplification transformed the problem from the sinusoidal signal domain into the phase signal domain, which simplified the problem of analyzing the PLL. It would be attractive if the same simplification could be done on the admittance model and the amplitude model.

Consider the case when a sinusoidal signal is acting on a general linear time invariant system S , with the transfer function $H(s)$. In stationarity the output is given by a sinusoidal signal with the same frequency, but with a different amplitude and a phase shift. The output $y(t)$ of the linear system, with the input signal $u(t) = u_0 \sin \omega t$, is thus given by

$$y(t) = |H(j\omega)|u_0 \sin(\omega t + \arg\{H(j\omega)\})$$

This statement can be transformed into the phase signal domain. Let $\theta_1(t) = \omega t$ be the phase of the input signal, and let $\theta_2(t) = \omega t + \arg\{H(j\omega)\}$ be the phase of the output signal. Figure 11(a) shows the relations between the input signal and the output signal in the sinusoidal signal domain, and Figure 11(b) shows the same relation in the phase signal domain. A new dynamical system $G(\theta)$ has been introduced to describe the dynamics of the system S in the phase signal domain.

With $\varphi(\omega) = \arg\{H(j\omega)\}$ the following expression is valid in *stationarity*

$$\theta_2(t) = \theta_1(t) + \varphi(\omega) \quad (19)$$

This expression leads to an important statement; *if the system S has reached stationarity, its influence in the phase signal domain is given by the system in Figure 12, where $\varphi(\omega)$ is the phase function for the system S .* Notice that this is only true when the linear system S has reached stationarity which implies that the transients in the phase signal domain has disappeared.

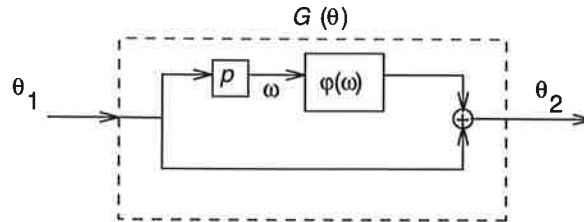


Figure 12. Stationary behavior of the system $G(\theta)$, where $p = \frac{d}{dt}$ is the differential operator.

Approximation of the Phase Signal Domain Dynamics

Still the dynamics of the system $G(\theta)$, that relates the input phase signal to the output phase signal in the phase signal domain, is not known. However, assuming that the dynamics of this system can be neglected, expression (19) is always true and the system $G(\theta)$ is approximated by the system in Figure 12, where $\varphi(\omega)$ is the phase function of the linear system. This gives the following important approximation; *if the dynamics of the system $G(\theta)$ in the phase signal domain is neglected, then the influence of the system S in the phase signal domain can be approximated by the stationary behavior of S in the phase signal domain, which is known. The approximation of $G(\theta)$ is given by the system in Figure 12.* Observe that the phase function does not contain any dynamics.

Summary

In this section a very important approximation was introduced. This approximation will later simplify the analysis of the PLL connected to a linear time invariant system. It can be expected that the validity of the approximation will be better for a damped system than a badly damped system, since the transients in the damped system will disappear much faster than the transients in the badly damped system.

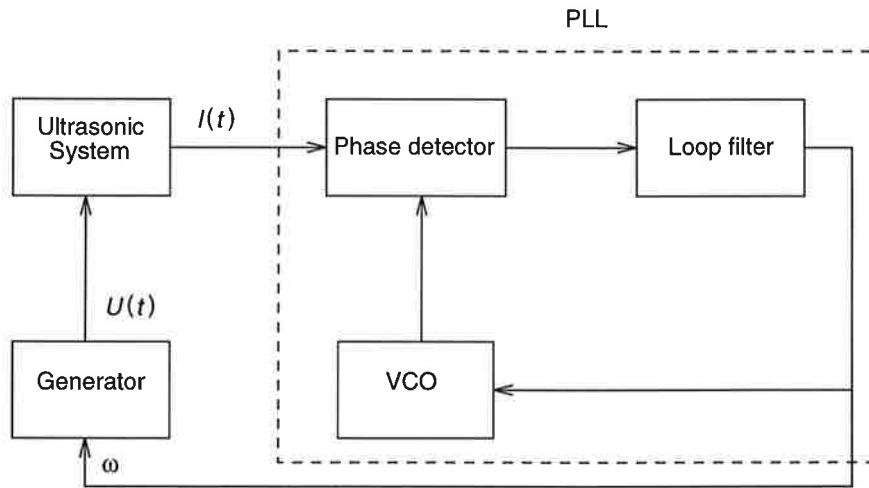


Figure 13. The existing setup of the PLL and the ultrasonic system.

7. Using the PLL with the Admittance Model

As mentioned earlier it is known that when the system works at its resonance frequency, the complex valued load seen from the generator becomes real valued. Thus the phase shift between the current and the voltage at the output of the generator becomes zero³. A possible control strategy is to use a PLL to keep the phase difference between the current and the voltage small, forcing the frequency of the generator to reach the resonance frequency of the system. When the phase shift between the current and the voltage is zero, all power produced by the generator will be delivered into the system. If the generator is working at the resonance frequency of the system, the current from the generator will become minimal, which can be seen in Figure 3.

Setup of the PLL with the Admittance Model

Figure 13 shows how to connect the PLL to the system. An extra output has been added to the PLL, which is used to control the frequency of the generator. The generator then produces a sinusoidal voltage $U(t)$ to the system with the frequency decided by the PLL. The resulting current $I(t)$ is thought of as the output signal from the system and input signal to the PLL, and a feedback is thus introduced. This is the strategy used to control the frequency of the generator in the existing equipment, and it has some advantages. First both the current and the voltage from the generator are easy to measure. Next there is no need to make any measurements at the stack, which works in an unfriendly environment. There are, however, some major drawbacks with this solution, which will be discussed later.

Transformation of the PLL/Admittance Model Setup

The new system has to be analyzed to see if there are any problems with stability due to the feedback. This analysis is very complicated because of the

³ Observe that this is true only when the generator and stack are perfectly matched, which is an unrealistic assumption. See the discussion later in Section 7.

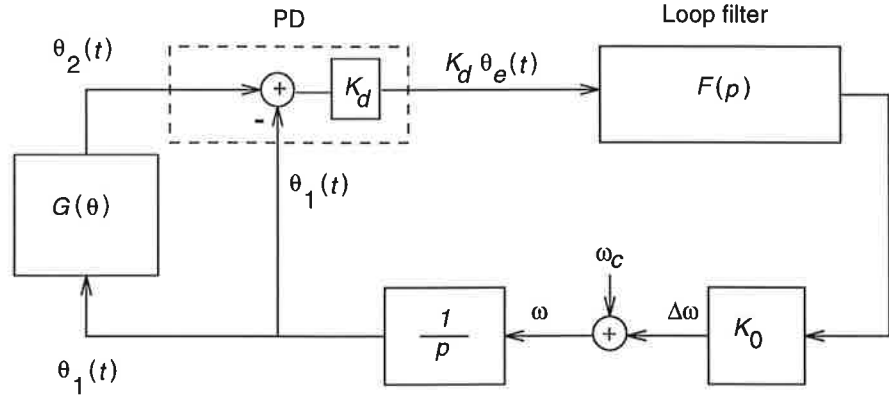


Figure 14. Linear model of the PLL connected to the ultrasonic system (in the phase signal domain).

lack of knowledge of the dynamics of the phase signals acting in the system. Although the dynamics of the system is known when sinusoidal voltage signals are used as input signals, the dynamics of the system in the phase signal domain is hard to determine analytically. Introducing $G(\theta)$ to describe the dynamics in the phase signal domain, the setup in Figure 13 can be transformed into the phase signal domain according to the discussion in Section 6. With $\omega = \omega_c + \Delta\omega$ the resulting system is shown in Figure 14, where $p = \frac{d}{dt}$ is the differential operator, ω_c is the center frequency of the PLL and $\Delta\omega$ is the frequency deviation from ω_c . Once again the phase error is assumed to be small, so the average output of the PD is approximately linear. In practice the center frequency is chosen as the nominal resonance frequency of the system, i.e. $\omega_c = \omega_0$.

Selection of the Loop Filter

There is one conclusion that can be drawn from studying the model of the PLL connected to the admittance model in Figure 14. First the assumption that the new feedback did not introduce any stability problems is made. Next it is assumed that the system $G(\theta)$ has reached stationarity. Rewriting (19) and introducing the phase error gives

$$\theta_e(t) = \theta_2(t) - \theta_1(t) = \varphi_{VI}(\omega)$$

Recalling the discussion in Section 5, where it was shown that the phase error in steady state depended on the type of loop filter used, it is now easy to choose loop filter. Since the filter of type 1 introduced a steady state phase error the phase shift $\varphi_{VI}(\omega)$ cannot equal zero. Instead $\varphi_{VI}(\omega) = \theta_e(\infty) \neq 0$ which implies that $\omega(\infty) \neq \omega_0$. Therefore an active loop filter of type 3 is chosen and used from now on. Since $\theta_e(\infty) = 0$ for this filter, no steady state frequency error will be introduced and $\omega(t) \rightarrow \omega_0$ when $t \rightarrow \infty$. Notice that this is true only if L_0 is correctly chosen, i.e. the generator and the stack are perfectly matched.

Approximation of the PLL/Admittance Model Setup

If the approximation of the system $G(\theta)$ from Section 6 is applied to the

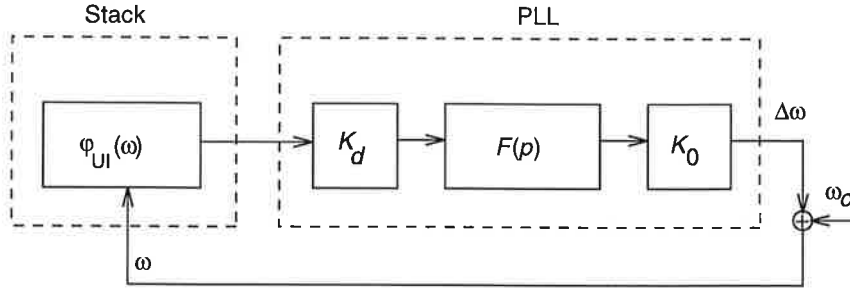


Figure 15. Block scheme for the frequency deviation behavior of the PLL.

system in Figure 14, a new simpler system is obtained. The approximation said that the system $G(\theta)$ could be replaced by the system in Figure 12. Since $\varphi_{UI}(\omega)$ only depends on the frequency, not the phase, decided by the PLL, the integrator can be removed from the block scheme in Figure 14. For the same reason the differentiation p in $G(\theta)$ is also removed. This gives a new block scheme that governs the behavior of the frequency deviation $\Delta\omega$ in the PLL/Admittance model setup, see Figure 15. From the new block scheme it is seen that the nonlinear differential equation for $\Delta\omega$ is given by

$$\Delta\omega - K_0 K_d F(p) \varphi_{UI}(\omega_c + \Delta\omega) = 0$$

A very important interpretation of this approximation is that *the behavior of the PLL is decided from the phase function of the system. If the phase function is positive the PLL decreases the frequency of the generator, and if the phase function is negative the frequency is increased.* This statement makes it possible to predict the PLL's behavior by examining the phase function of the system to which the PLL is connected.

Problems with the PLL/Admittance Model Setup

Three major problems appear when using the PLL together with the system.

The first one has to do with the matching of the generator and stack. It was shown in Section 2 how to choose L_0 in order to get zero phase shift between the current and the voltage from the generator at the resonance frequency. The expression included three, in practice, time varying parameters. Due to this variation in parameters the generator will never be well matched, i.e. the phase shift between voltage and current will *not* be zero at the system's resonance frequency. Instead the phase shift will become zero at some other frequency, and it is at this frequency the PLL will lock. This implies that the generator will not work at the system's resonance frequency, although the phase shift between the current and voltage from the generator is zero.

The second problem occurs when the system is working under high pressure, causing R to increase. The pressure is an important parameter that affects the quality of the sealing. Mostly high pressure is wanted, which corresponds to a high R . For high R the phase function will degenerate, which makes it impossible for the PLL to find the resonance frequency. The degenerated phase function is shown in Figure 16, and it is seen that the slope of the phase function has changed sign. Because of this the PLL will drift either

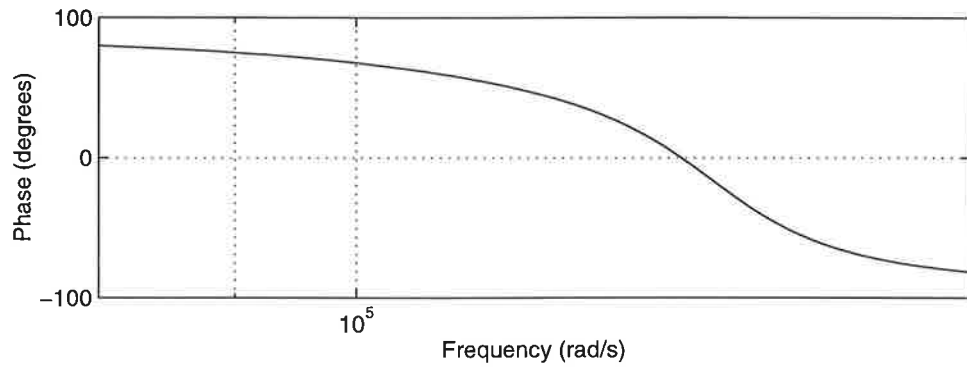


Figure 16. Degenerated phase function due to high pressure, and the PLL will never be able to lock. Parameter values used: $C_0 = 15.8$ nF, $C = 2.18$ nF, $R = 3000$ Ω , $L = 29.7$ mH and $L_0 = 3.6$ mH.

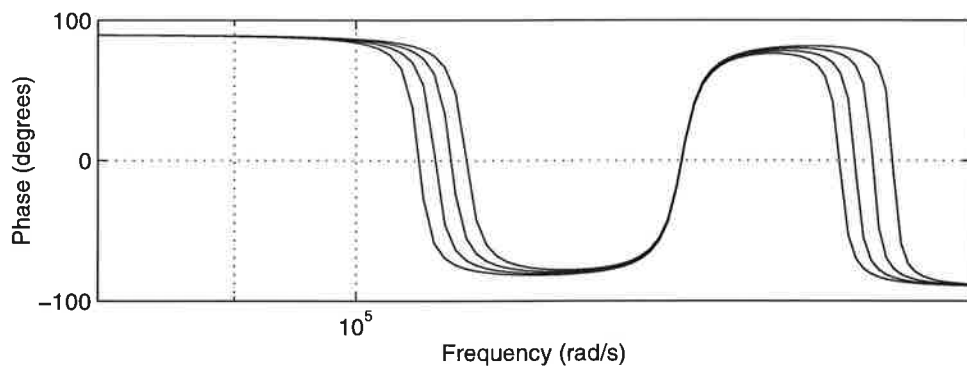


Figure 17. Phase function when R is small. The badly chosen L_0 does not affect the resonance frequency, and the PLL will always be able to lock. Parameter values used: $C_0 = 15.8$ nF, $C = 2.18$ nF, $L = 29.7$ mH, $R = 100$ Ω and $L_0 = 3.6 \pm 10\%$ mH.

towards lower or higher frequencies, depending on the frequency of the VCO when the phase function degenerated.

If the two problems are combined, i.e. L_0 is badly chosen and R is high, the problem with the mismatched generator becomes worse. The system now tolerates much less deviation of L_0 . In Figure 17 the phase function is shown for a fixed small R . The coil L_0 is varied $\pm 10\%$ around its nominal value. It is seen that the resonance frequency is not affected by L_0 . If R is increased, problems will occur. This phenomena is shown in Figure 18 where the phase function is drawn for several different L_0 with a constant high R . L_0 is varied $\pm 10\%$ around its nominal value, and it is clearly seen that for some combinations of L_0 and R the PLL will not be able to lock since the phase function never reaches zero. These cases are drawn in a dashed line style.

Practical experience shows that these problems do occur, specially when the stack is started up. The stack is then very damped, i.e. R is high, and the problems described above prevents successful frequency control. If, however, none of the problems presented above are present during the start up of the stack, the PLL will mostly have no problem to control the frequency of the generator. An interpretation of this is that when the stack is in motion, R is decreased and the problems presented above will not occur.

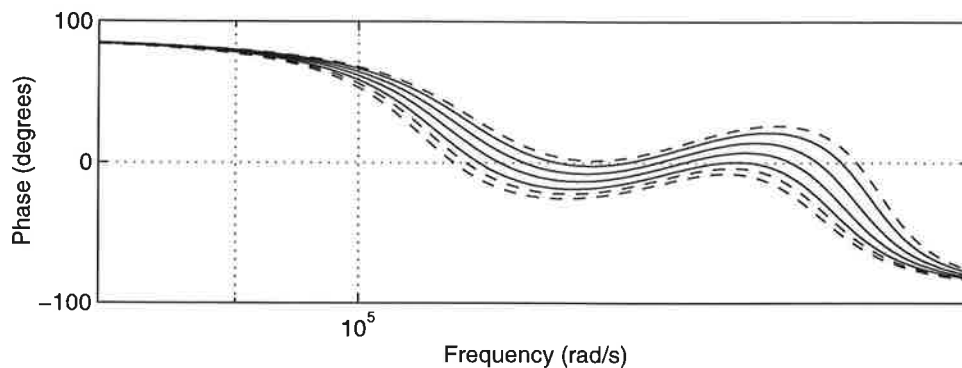


Figure 18. Degenerated phase function due to high pressure and mismatched L_0 . The solid curves shows the cases where the PLL is able to lock, and the dashed curves shows the cases where the PLL is *not* able to lock. Parameter values used: $C_0 = 15.8$ nF, $C = 2.18$ nF, $L = 29.7$ mH, $R = 1000$ Ω and $L_0 = 3.6 \pm 10\%$ mH.

The third problem treats the start up frequency of the PLL. If the start up frequency is chosen *outside* the two resonances of the admittance, the PLL will never be able to lock. If the start up frequency was chosen too high, the PLL will drift towards higher frequencies and if the frequency is chosen to low the PLL will drift towards lower frequencies. This can be seen in Figure 17.

Summary

In this section the existing solution to the control problem was examined. First the PLL and the admittance model was transformed into the phase signal domain. This transformation lead to the choice of an active loop filter. Via the transformation an important approximation were derived; the phase function of the system, to which the PLL is connected, can be used to determine the total system's behavior.

This approximation made it possible to discuss some of the problems with the existing equipment, and the problems discussed were

- Mismatched generator and stack
- Degeneration of the phase function due to high R
- The combination of the mismatch and high R
- The startup frequency of the generator

Since the solution of the frequency control problem presented above is implemented, some practical experience exists. The major problem is that the solution works well for small R , but it is preferable to operate the system under conditions when R is high. In practice problems when R has become to high has been encountered. It is therefore preferable to find a new solution to the frequency control problem of the generator, which works well for high R .

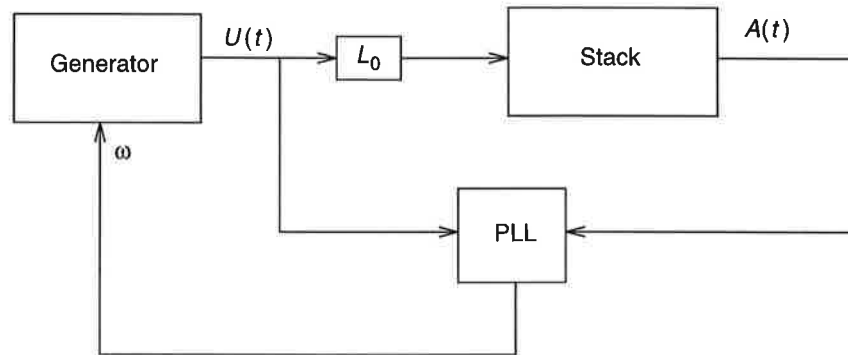


Figure 19. Amplitude feedback via the PLL.

8. Using the PLL with the Amplitude Model

It was shown in Section 7 that there were two major problems when using the PLL with the admittance model, badly chosen L_0 and the change of sign of $\frac{d\varphi_{VT}}{d\omega}$ when R was high. There were also a third problem with the start up frequency of the generator. One possible way to get around these problems is to measure the amplitude of the converter. It is realistic to assume that this measurement will give more information about the system than only measuring the generator current. Some of the problems presented previously will therefore hopefully be avoided.

The control strategy is to use a PLL to keep the phase shift between the output voltage from the generator and the amplitude of the converter small. In Figure 4 it is seen that the phase shift is zero at the resonance frequency (if L_0 is correctly chosen), and the PLL will guide the generator towards the resonance frequency of the system.

Setup of the PLL with the Amplitude Model

Figure 19 shows how to connect the PLL when using the amplitude of the converter as feedback. The PLL is used to control the frequency of the output voltage from the generator. If the phase shift between the generator voltage and the amplitude of the converter is zero, the generator is working at the system's resonance frequency. Notice that this is true only if the generator and stack are perfectly matched. Otherwise the frequency point where the phase shift is zero will *not* be the resonance frequency, instead the phase shift will be zero when $\omega = \frac{1}{\sqrt{L_0 C_0}}$. This new setup has several advantages to the admittance setup and these will be discussed later. The disadvantage of this method is mainly the need to measure the amplitude of the converter, which may be a nontrivial task.

It is worth noticing that it is irrelevant if the acceleration, velocity or the amplitude of the converter is measured. Their phase functions only differ by $\pi/2$ radians, which can be compensated for in the PLL.

For practical reasons it may be difficult to make the measurements at the physical point which corresponds to the point in the model, for which the amplitude model is derived. This means that the measurements may have to be made at some distance from the desired measurement point.

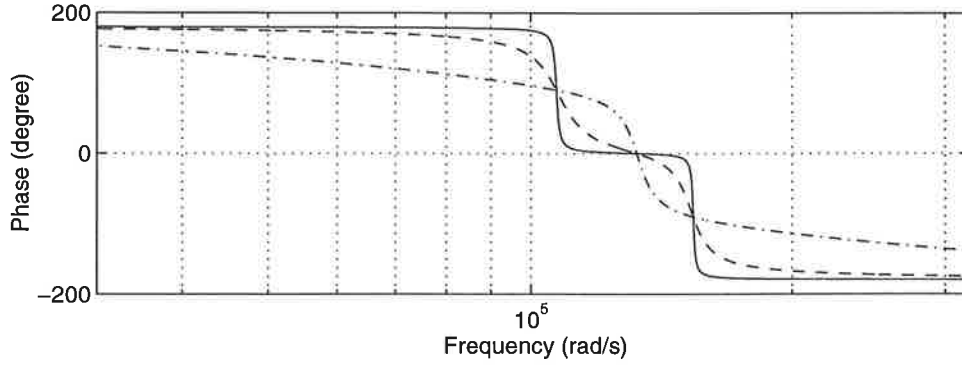


Figure 20. Phase function of $-H_{UA}(s)$ for different R . Solid line: $R = 70 \Omega$, dashed line: $R = 700 \Omega$ and dashed-dotted line: $R = 7000 \Omega$.

Properties of the Amplitude Model

The relation between the voltage of the generator and the amplitude of the converter was previously derived, and the resulting transfer function is given by (8). This model has some interesting properties. Assuming that the generator and the stack are perfectly matched, the calculations in Section 2 showed that $H_{UA}(s)$ was independent of R at the resonance frequency. This may seem like a paradox, but the admittance model shows that the generator has to increase the current delivered to the system to maintain the constant amplitude of the converter. In Figure 20 the phase function of $-H_{UA}(s)$ is plotted for different R .

Furthermore the sign of slope of the phase function for $H_{UA}(s)$ is independent of R (see Figure 20), so that problem is removed. This means that a PLL can be used to keep $\varphi_{UA}(\omega)$ small, thus forcing the frequency of the generator to reach the resonance frequency of the system. If the phase detector of the PLL is able to handle phase errors in the range $-\pi \leq \theta_e \leq \pi$, the PLL will always find the point where the phase curve is zero, independent of the start up frequency of the PLL.

Transformation of the PLL/Amplitude Model Setup

Recalling the discussion in Section 6 and assuming that the generator and stack are perfectly matched, the system in Figure 19 can be transformed into the phase signal domain analogously with the transformation in Section 7. This gives the system shown in Figure 21, where $G_1(p)$ contains the transformed PLL, i.e.

$$G_1(p) = \frac{K_0 K_d}{\tau_1} \frac{1 + \tau_2 p}{p}$$

and (see Section 7)

$$\omega = \omega_c + \Delta\omega$$

The equation describing the frequency deviation is given by

$$\Delta\omega - G_1(p)\varphi_{UA}(\omega_c + \Delta\omega) = 0$$

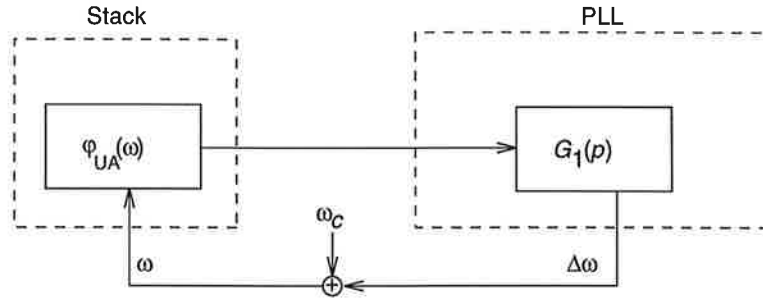


Figure 21. Transformation of the PLL/amplitude system into the phase signal domain.

This system could be simplified by a linearization of $\varphi_{UA}(\omega)$ around

$$\omega_0^0 = \omega_c = \sqrt{\frac{C_0 + C}{LCC_0}}$$

The derivative of the phase function in this point is given by

$$\left. \frac{d\varphi_{UA}}{d\omega} \right|_{\omega=\omega_0^0} = -2RC_0$$

and the linearization of $\varphi_{UA}(\omega)$ is thus given by

$$\varphi_{UA}^0(\omega) = -2RC_0\omega$$

With this linear function the differential equation that describes the frequency deviation turns into

$$\frac{d\Delta\omega}{dt} + \frac{1}{\frac{\tau_1}{K_0K_dRC_0} + \tau_2}(\omega_c + \Delta\omega) = 0$$

This equation gives a rough estimation of the frequency deviation $\Delta\omega$ of the amplitude model. It can also be used to give a hint about how to choose the parameters in the PLL. It is easily seen that the differential equation's behavior is decided by the pole

$$s = -\frac{1}{\frac{\tau_1}{K_0K_dRC_0} + \tau_2} \quad (20)$$

and the system will be stable for $s < 0$. Notice, however, that pole placement will not give unique parameters in the PLL since only one constraint is used to determine the three parameters K_0 , τ_1 and τ_2 .

Adaptation of the Coil L_0

Still the problem with the mismatch of the generator and the stack, due to parameter variations, exists. The PLL will regulate the frequency towards the frequency where $\varphi_{UA}(\omega) = 0$, i.e.

$$\omega = \frac{1}{\sqrt{L_0C_0}}$$

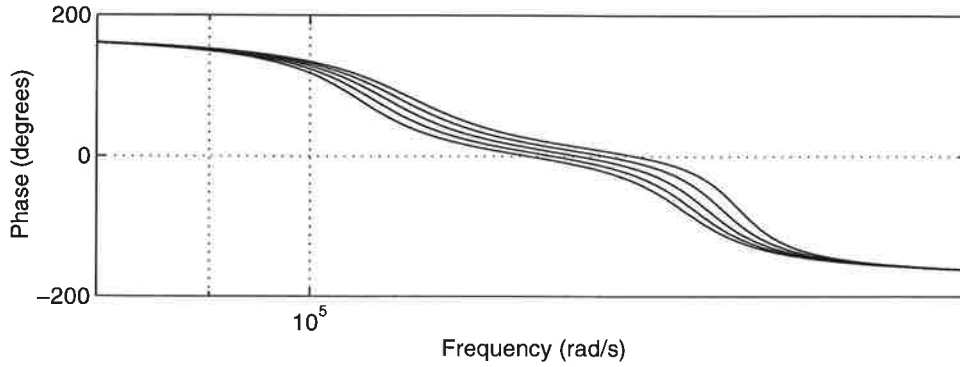


Figure 22. Influence of L_0 on $\varphi_{UA}(\omega)$ when L_0 is varied $\pm 10\%$ around its nominal value 3.6 mH. Parameter values used: $C_0 = 15.8$ nF, $C = 2.18$ nF, $R = 1000$ Ω and $L = 29.7$ mH.

If L_0 is not correctly chosen this ω will *not* be the resonance frequency of the system. The problem with mismatched generator and stack has even become worse compared to the PLL/admittance model setup, where the problem only become obvious when R was high (see Figure 17 and Figure 18). The frequency deviation from the resonance frequency is now independent of R , which means that the problem is present for all R . In Figure 22 the influence of different L_0 on $\varphi_{UA}(\omega)$ is shown. L_0 is varied $\pm 10\%$ around its nominal value. This figure shows that it is preferable to adjust the coil L_0 in some way so that the generator will be well matched to the stack during the whole sealing cycle.

Since the current from the generator is not used for frequency regulation any longer, this signal can be used to adjust L_0 . It can be expected that it will be necessary to adjust $L_0 \pm 10\%$ due to the temperature dependence in C_0 . Measuring the phase shift between the current and the voltage from the generator gives an indication of how well matched the generator and the stack are. This phase shift can be used to adjust L_0 in such a way that the phase shift becomes smaller. At the same time the amplitude feedback via the PLL will regulate the frequency of the generator. The new setup is shown in Figure 23.

Transformation of the L_0 Adjustment Setup

In order to analyze the setup in Figure 23 the system has to be transformed into the phase signal domain. Introduce $G_1(s)$ to describe the dynamics of the PLL and $G_2(s)$ to describe the dynamics of the not yet determined update law of L_0 , consisting of the low pass filter and the adjustment of L_0 . The approximation introduced in Section 6 gives the transformed system in Figure 24. This new setup includes two nonlinear functions, $\varphi_{VI}(\omega, L_0)$ and $\varphi_{VA}(\omega, L_0)$.

Investigation of Equilibrium Points

The adjustment of L_0 and the amplitude feedback via the PLL will affect each other, and it is important to prove that the adjustment of L_0 does not introduce any stability problems. Because of the complex mathematical structure of this problem this is not easily done. There are however one necessary condition for stability that can be checked. If the frequency regulation and the L_0 adjustment is successful, the system must reach an equilibrium point where

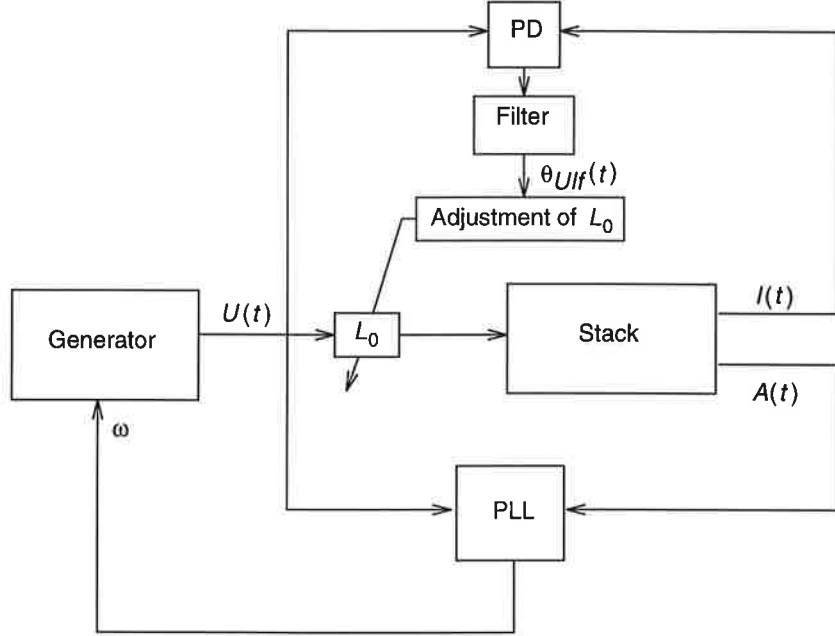


Figure 23. Amplitude feedback via the PLL with adjustment of L_0 .

both the phase shift between the amplitude and the voltage and the current and the voltage is zero, i.e.

$$\begin{cases} \varphi_{UI}(\omega, L_0) = \arg \{H_{UI}(j\omega)\} = 0 \\ \varphi_{UA}(\omega, L_0) = \arg \{-H_{UA}(j\omega)\} = 0 \end{cases} \quad (21)$$

The point where this constraint is fulfilled should be

$$\begin{cases} \omega = \omega_0^0 = \sqrt{\frac{C_0 + C}{LCC_0}} \\ L_0 = L_0^0 = \frac{CL}{C_0 + C} \end{cases} \quad (22)$$

which is the point where the generator and stack are perfectly matched and the generator is working at the resonance frequency of the system.

Rewriting the admittance transfer function (1) gives

$$H_{UI}(s) = \frac{\frac{1}{L_0} s \left(s^2 + \frac{R}{L} s + \frac{C_0 + C}{LCC_0} \right)}{s^4 + \frac{R}{L} s^3 + \left(\frac{1}{LC} + \frac{L_0 + L}{C_0 LL_0} \right) s^2 + \frac{R}{C_0 LL_0} s + \frac{1}{CC_0 LL_0}}$$

which can be compared to the transfer function (8) of the amplitude model. Subtracting the two equations in (21) from each other gives

$$\arg \{H_{UI}(j\omega)\} - \arg \{-H_{UA}(j\omega)\} = 0$$

Since the denominators of $H_{UI}(j\omega)$ and $-H_{UA}(j\omega)$ are equal, the problem turns into determining the frequencies ω where

$$\arg \left\{ j\omega \left((j\omega)^2 + \frac{R}{L} j\omega + \frac{C_0 + C}{LCC_0} \right) \right\} - \arg \left\{ -\frac{1}{C_0 L} \right\} = 0$$

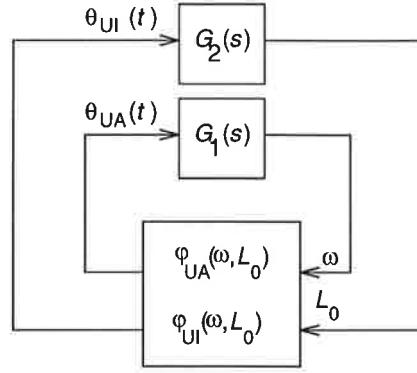


Figure 24. Transformation of the PLL/adaptive amplitude model into the phase signal domain.

which can be simplified to

$$\arg \left\{ (j\omega)^2 + \frac{R}{L}j\omega + \frac{C_0 + C}{LCC_0} \right\} = \frac{\pi}{2}$$

Introducing the resonance frequency $\omega_0 = \sqrt{\frac{C_0 + C}{LCC_0}}$ and the damping $\zeta = \frac{R}{2L\omega_0}$ it is realized that the phase shift is $\pi/2$ at the resonance frequency as long as the damping $\zeta < 1$, that is

$$\zeta = \frac{R}{2L\omega_0} < 1 \Rightarrow R < 2\sqrt{\frac{L(C_0 + C)}{CC_0}}$$

and under this condition there exists only one equilibrium point. For a normal system the constraint gives $R < 8 \cdot 10^3$, which can be regarded as a very high R . If $\zeta > 1$ there will still be a frequency point where the phase shift equals $\pi/2$ but that point will not be the resonance frequency.

Left to show is that there is only one L_0 that fulfills (22). This is done by solving for L_0 in

$$\varphi_{UA}(\omega_0^0, L_0) = 0$$

which gives

$$\frac{1}{L_0 C_0} - (\omega_0^0)^2 = 0$$

which have the unique solution

$$L_0 = \frac{CL}{C_0 + C} = L_0^0$$

Thus the existence of an unique equilibrium point (ω_0^0, L_0^0) is guaranteed if the constraint on R is fulfilled. Observe that the constraint on R is only a nessecary condition for stability. The system may be unstable even if the constraint on R is fulfilled.

Linearization of the PLL/Adaptive Amplitude Model Setup

Figure 25 shows the two phase functions $\varphi_{UI}(\omega, L_0)$ and $\varphi_{UA}(\omega, L_0)$, and it is seen that these functions are almost linear around the equilibrium point. If

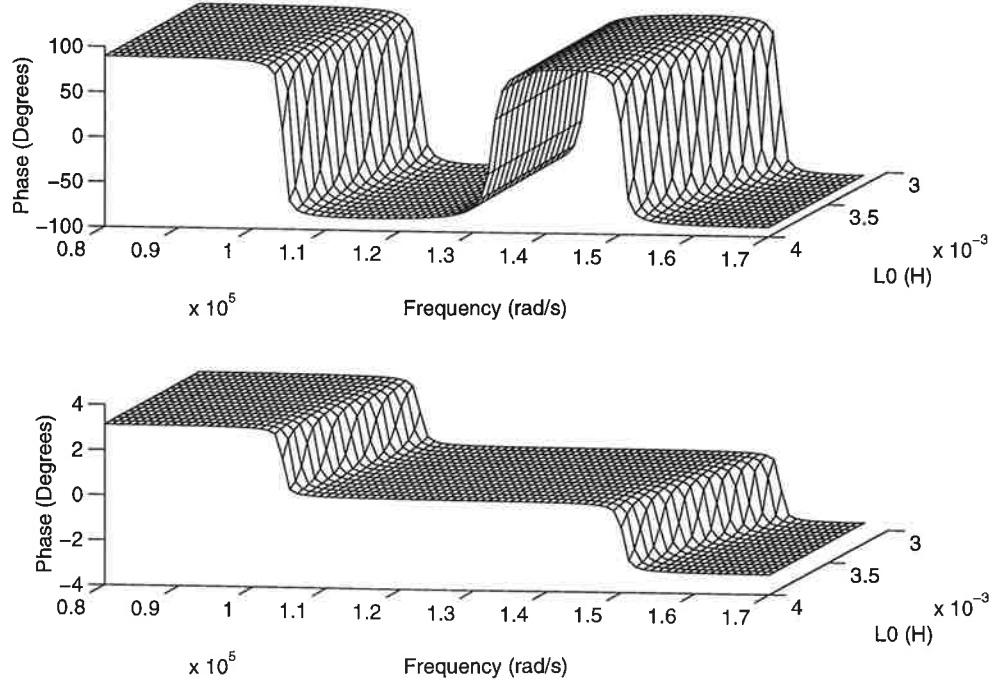


Figure 25. Motivation of the linearization. $\varphi_{UI}(\omega, L_0)$ is shown in the upper plot and $\varphi_{UA}(\omega, L_0)$ is shown in the lower plot. Parameter values used: $C_0 = 15.8$ nF, $C = 2.18$ nF, $R = 50$ Ω and $L = 29.7$ mH. This gives $\omega_0^0 = 132574$ rad/s and $L_0^0 = 3.6$ mH.

the system in Figure 24 is linearized around the equilibrium point (22), i.e. the two nonlinear functions $\varphi_{UI}(\omega, L_0)$ and $\varphi_{UA}(\omega, L_0)$ are linearized around (ω_0^0, L_0^0) , a new linear system is obtained. Introduce the gain matrix

$$K = \begin{bmatrix} k_{11} & k_{12} \\ k_{21} & k_{22} \end{bmatrix} = \begin{bmatrix} -\frac{\partial \varphi_{UA}}{\partial \omega} & -\frac{\partial \varphi_{UA}}{\partial L_0} \\ -\frac{\partial \varphi_{UI}}{\partial \omega} & -\frac{\partial \varphi_{UI}}{\partial L_0} \end{bmatrix} = \begin{bmatrix} 2RC_0 & \frac{RC_0\omega_0^0}{L_0^0} \\ -2\frac{L - C_0R^2}{R} & \frac{RC_0\omega_0^0}{L_0^0} \end{bmatrix}$$

and the transfer function matrix

$$G(s) = \begin{bmatrix} G_1(s) & 0 \\ 0 & G_2(s) \end{bmatrix}$$

The linearization of the system in Figure 24 is then given by Figure 26, where some new signals have been introduced. Their Laplace transforms are given by

$$N(s) = \mathcal{L}\{n(t)\} = \begin{bmatrix} N_1(s) \\ N_2(s) \end{bmatrix}$$

$$\Theta(s) = \mathcal{L}\{\theta(t)\} = \begin{bmatrix} \Theta_{UA}(s) \\ \Theta_{UI}(s) \end{bmatrix}$$

$$L_0(s) = \mathcal{L}\{L_0(t)\}$$

$$\Omega(s) = \mathcal{L}\{\omega(t)\}$$

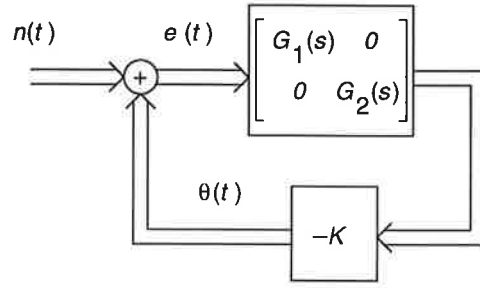


Figure 26. Linearization of the PLL/amplitude model setup with adjustment of L_0 .

where $\theta(t) = [\theta_{UA}(t) \quad \theta_{UI}(t)]^T$ contains the two phase errors in the system, and $n(t) = [n_1(t) \quad n_2(t)]^T$ is an external signal only used to analyze this setup. It will later be set equal to zero. This gives the following relation between the input signal and the error

$$E(s) = N(s) - \Theta(s) = N(s) - KG(s)E(s)$$

or

$$E(s) = (I + KG(s))^{-1}N(s)$$

With $G_1(s) = B_1(s)/A_1(s)$ and $G_2(s) = B_2(s)/A_2(s)$ matrix calculations gives

$$\begin{aligned} E(s) &= (I + KG(s))^{-1}N(s) = \left[I + K \begin{bmatrix} \frac{B_1(s)}{A_1(s)} & 0 \\ 0 & \frac{B_2(s)}{A_2(s)} \end{bmatrix} \right]^{-1} N(s) \\ &= \frac{1}{\alpha(s)} \begin{bmatrix} A_1A_2 + k_{22}A_1B_2 & -k_{12}A_1B_2 \\ -k_{21}A_2B_1 & A_1A_2 + k_{11}A_2B_1 \end{bmatrix} N(s) \end{aligned} \quad (23)$$

where

$$\alpha(s) = A_1A_2 + k_{22}A_1B_2 + k_{11}A_2B_1 + (k_{11}k_{22} - k_{12}k_{21})B_1B_2$$

Assuming that (23) is stable the final value theorem can be applied. Let $n(t)$ be a step disturbance ($N(s) = \mathcal{L}\{n(t)\} = \Delta N/s$), and the stationary error is given by

$$\lim_{t \rightarrow \infty} e(t) = \lim_{s \rightarrow 0} s(I + KG(s))^{-1} \frac{\Delta N}{s} = \lim_{s \rightarrow 0} (I + KG(s))^{-1} \Delta N$$

where $\Delta N = [\Delta N_1 \quad \Delta N_2]^T$. Assuming that the limit exists gives

$$e(\infty) = \begin{bmatrix} A_1(0)A_2(0) + k_{22}A_1(0)B_2(0) & -k_{12}A_1(0)B_2(0) \\ -k_{21}A_2(0)B_1(0) & A_1(0)A_2(0) + k_{11}A_2(0)B_1(0) \end{bmatrix} \frac{\Delta N}{\alpha(0)}$$

It is now seen that if both $G_1(s)$ and $G_2(s)$ contains an integrator then $A_1(0) = 0$ and $A_2(0) = 0$ and the limit turns into

$$\lim_{t \rightarrow \infty} e(t) = \begin{bmatrix} 0 \\ 0 \end{bmatrix}$$

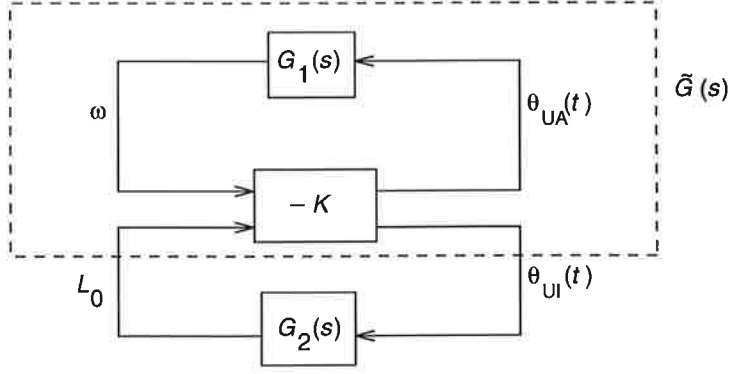


Figure 27. Reorganization of the PLL/amplitude setup with L_0 adjustment. The reorganization is made to be able to choose $G_2(s)$.

There will be no stationary phase error if integrators are inserted into $G_1(s)$ and $G_2(s)$. If these two transfer functions does not contain any integrators, a stationary phase error will occur. In the limit the value of $\alpha(0) \neq 0$ because $B_1(0)B_2(0) \neq 0$, which shows that the matrix inversion made previously is valid. The result shows that $G_1(s)$ must include an integrator, i.e. the PLL must have an active loop filter, as stated in Section 7.

The main characteristics of this multivariable system is given by the poles of the system, which can be determined from

$$\alpha(s) = 0$$

or

$$A_1A_2 + k_{22}A_1B_2 + k_{11}A_2B_1 + (k_{11}k_{22} - k_{12}k_{21})B_1B_2 = 0 \quad (24)$$

Design of the L_0 Adjustment Controller

Still there is a need to choose $G_2(s) = B_2(s)/A_2(s)$ so that the total system will behave in a desired way. The only constraint on $G_2(s)$ is that it has to contain an integrator. If the transfer function from $L_0(s)$ to $\Theta_{UI}(s)$ is calculated an ordinary *SISO* system is obtained, and $G_2(s)$ can be designed with standard control theory design methods.

Once again the system is reorganized in a way that is convenient for the problem formulation. This new form is shown in Figure 27. It is known that

$$\begin{bmatrix} \Theta_{UA}(s) \\ \Theta_{UI}(s) \end{bmatrix} = -K \begin{bmatrix} \Omega(s) \\ L_0(s) \end{bmatrix} = - \begin{bmatrix} k_{11}\Omega(s) + k_{12}L_0(s) \\ k_{21}\Omega(s) + k_{22}L_0(s) \end{bmatrix} \quad (25)$$

and Figure 27 gives

$$\Omega(s) = G_1(s)\Theta_{UA}(s) = -G_1(s)(k_{11}\Omega(s) + k_{12}L_0(s))$$

or

$$\Omega(s) = -\frac{k_{12}G_1(s)}{1 + k_{11}G_1(s)}L_0(s)$$

Substituting this expression for $\Omega(s)$ into (25) gives the dynamics between $L_0(s)$ and $\Theta_{UI}(s)$,

$$\Theta_{UI}(s) = k_{21}\Omega(s) + k_{22}L_0(s) = \left(-\frac{k_{12}k_{21}G_1(s)}{1 + k_{11}G_1(s)} + k_{22} \right) L_0(s) = \tilde{G}(s)L_0(s)$$

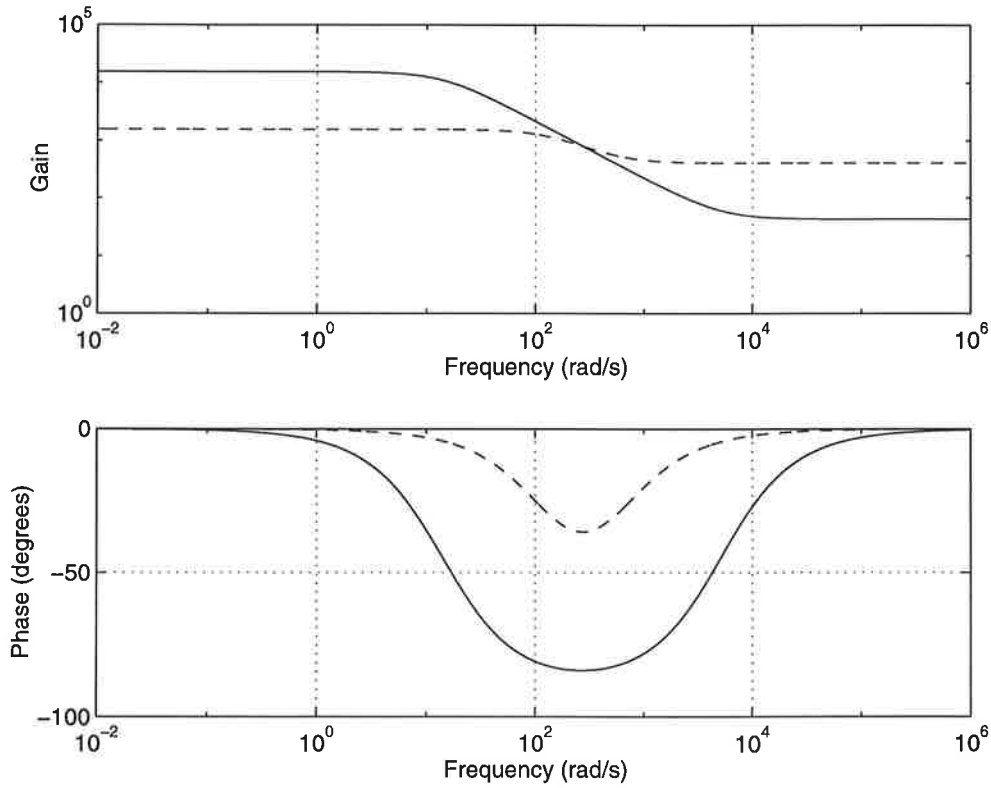


Figure 28. Bode plot for $\tilde{G}(s)$ with $R = 70 \Omega$ (solid line) and $R = 700 \Omega$ (dashed line). Other parameter values used: $C_0 = 15.8 \text{ nF}$, $C = 2.18 \text{ nF}$, $L_0 = 3.6 \text{ mH}$ and $L = 29.7 \text{ mH}$.

In Figure 28 the bode plot for $\tilde{G}(s)$ is shown for two different R .

It is now possible to derive a design method for determination of $G_1(s)$ and $G_2(s)$. Since the structure of $G_1(s)$ is known and given by

$$G_1(s) = \frac{K_0 K_d}{\tau_1} \frac{1 + \tau_2 s}{s} = d \frac{1 + \tau_2 s}{s}$$

only the constants $d = K_0 K_d / \tau_1$ and τ_2 has to be determined. This can be done by tuning these parameters for the system without any adaptation of L_0 . The behavior of that system is given by the location of the pole in expression (20). Now $G_1(s)$ is completely known and $G_2(s)$ can be designed so that the closed loop system in Figure 27 will behave in a specified manner. The only constraint on $G_2(s)$ is that it has to include an integrator. The locations of the poles of the closed loop system is given by (24).

One choice of the update law of L_0 is

$$\frac{dL_0}{dt} = \gamma \theta_{UIf}(t)$$

or

$$L_0(t) = \gamma \int_0^t \theta_{UIf}(\tau) d\tau + L_0(0)$$

where $\theta_{UIf}(t)$ is the low pass filtered phase error between the current and voltage from the generator, γ is the *adjustment gain* and $L_0(0)$ is the initial

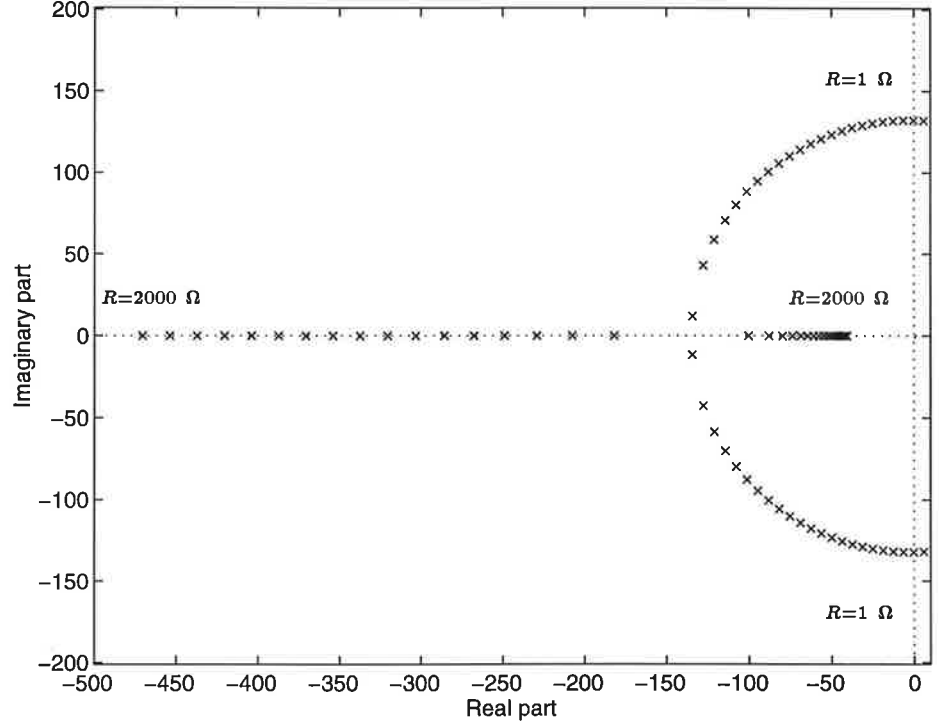


Figure 29. Root locus when using the first update law. R is varied in steps of 50Ω from $R = 1 \Omega$ to $R = 2000 \Omega$. Parameter values used: $K_0 = 10000$, $K_d = 2/\pi$, $\tau_1 = 0.001$, $\tau_2 = 10^{-5}$, $a = 1/0.0007$, $\gamma_1 = 0.001$ and $\gamma_2 = 0.08$.

value of L_0 . With this update law and with the low pass filter, $G_2(s)$ is given by

$$G_2(s) = \frac{a}{s} \frac{\gamma}{s + a}$$

It is seen that $G_2(s)$ contains an integrator. With this choice of $G_2(s)$ the closed loop system will behave well when the system is working under pressure. If R becomes too small instability problems will occur. This can be seen in Figure 29 where the locations of the poles, given by (24), is plotted for different R . In the plot R is varied from $R = 1 \Omega$ to $R = 2000 \Omega$ in steps of 50Ω . For small R there are two poles in the right half plane, indicating that the linearized system is unstable. When R grows, the poles are moved into the left half plane and the system becomes stable. The third pole of the system is located far into the left half plane and omitted from the plot.

One way to get around the instability problem is to choose another update law. If the previous update law of L_0 is modified with a proportional term, a new update law is given by

$$L_0(t) = \gamma_1 \theta_{UIf}(t) + \gamma_2 \int_0^t \theta_{UIf}(\tau) d\tau + L_0(0)$$

or

$$\frac{dL_0}{dt} = \gamma_1 \frac{d\theta_{UIf}}{dt} + \gamma_2 \theta_{UIf}(t) \quad (26)$$

where γ_1 and γ_2 are adjustment gains. This update law (with the low pass

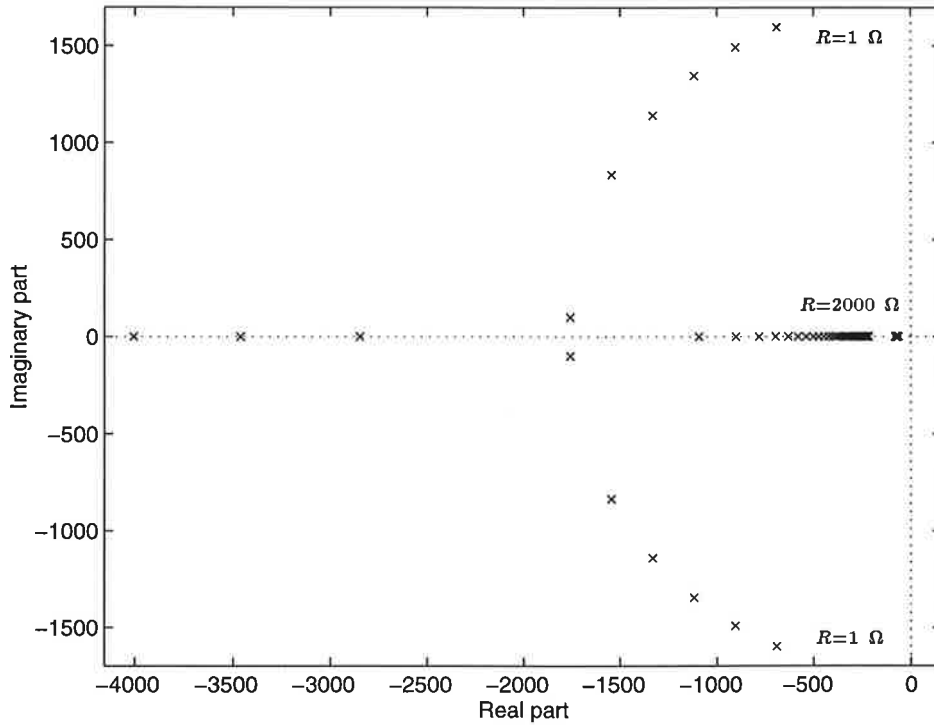


Figure 30. Root locus when using the modified update law. R is varied in steps of 50Ω from $R = 1 \Omega$ to $R = 2000 \Omega$. Parameter values used: $K_0 = 10000$, $K_d = 2/\pi$, $\tau_1 = 0.001$, $\tau_2 = 10^{-5}$, $a = 1/0.0007$, $\gamma_1 = 0.01$ and $\gamma_2 = 0.8$.

filter after the PD included) will give

$$G_2(s) = \frac{a}{s + a} \left(\gamma_1 + \frac{\gamma_2}{s} \right)$$

which contains an integrator. The instability problem for small R is now removed, which can be seen in the root locus in Figure 30. In this root locus the poles are always located in the left half plane, even for small R which correspond to the complex conjugated poles. When R is increased the poles will approach the real axis. The third pole is now located near the origin, which is better seen in Figure 31. It is seen that the location of the pole does not depend much on R , and it is this pole that will dominate the behavior of the system.

The discussion on how to choose $G_2(s)$ shows that *the choice of $G_2(s)$ is of great importance for the behavior of the total system*. It is probably easy to find a $G_2(s)$ that will give the total system a better performance than the $G_2(s)$ chosen above.

Summary

In this section a new approach to the control problem was taken. A feedback from the amplitude of the converter via a PLL was introduced. This feedback eliminated the problems with the degenerated phase function and startup frequency.

The problem with the mismatched generator and stack was however not removed. With amplitude feedback it has become even worse, since the prob-

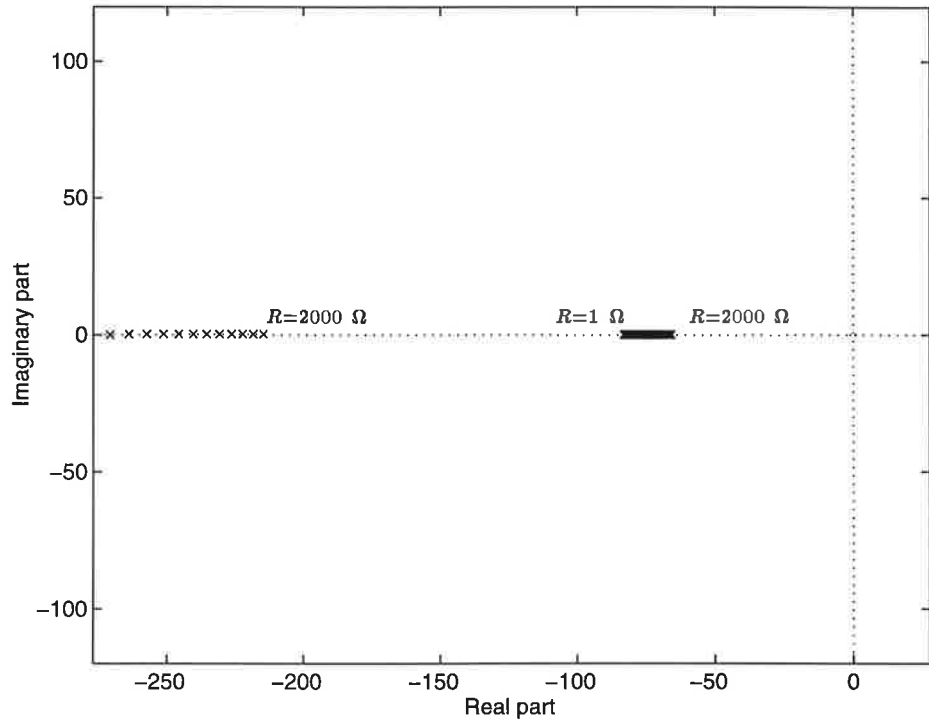


Figure 31. Magnified root locus when using the modified update law. The third pole is now seen and it is not much affected by R . As before R is varied in steps of 50Ω from $R = 1 \Omega$ to $R = 2000 \Omega$. Parameter values used: $K_0 = 10000$, $K_d = 2/\pi$, $\tau_1 = 0.001$, $\tau_2 = 10^{-5}$, $\alpha = 1/0.0007$, $\gamma_1 = 0.01$ and $\gamma_2 = 0.8$.

lem is now present for all R . Therefore an update law for L_0 was introduced, which should try to adjust L_0 in such a way that the generator and stack always are well matched. The update of L_0 was based on the phase shift between the current and voltage from the generator, which gives an indication of how well matched the generator and stack are.

A design method was derived, which consisted of two steps. First the parameters of the PLL was chosen independent of the adjustment of L_0 . Secondly an update law was chosen, regarding the parameters in the PLL as fixed. One important constraint on the design is that both the PLL and the update law of L_0 has to include an integrator, in order to avoid stationary phase errors.

All analysis and design was made in the phase signal domain with the two phase functions linearized around the resonance frequency and the nominal value of L_0 .

Two different update laws were proposed, and it was shown that there will be stability problems with the first one if R is too small. Under normal working conditions it will however work satisfactory. With the second update law of L_0 the instability problem with small R was removed. The reason for investigation of two different $G_2(s)$ is to show that it is important how $G_2(s)$ is chosen. More work is needed to find an optimal $G_2(s)$ for implementation.

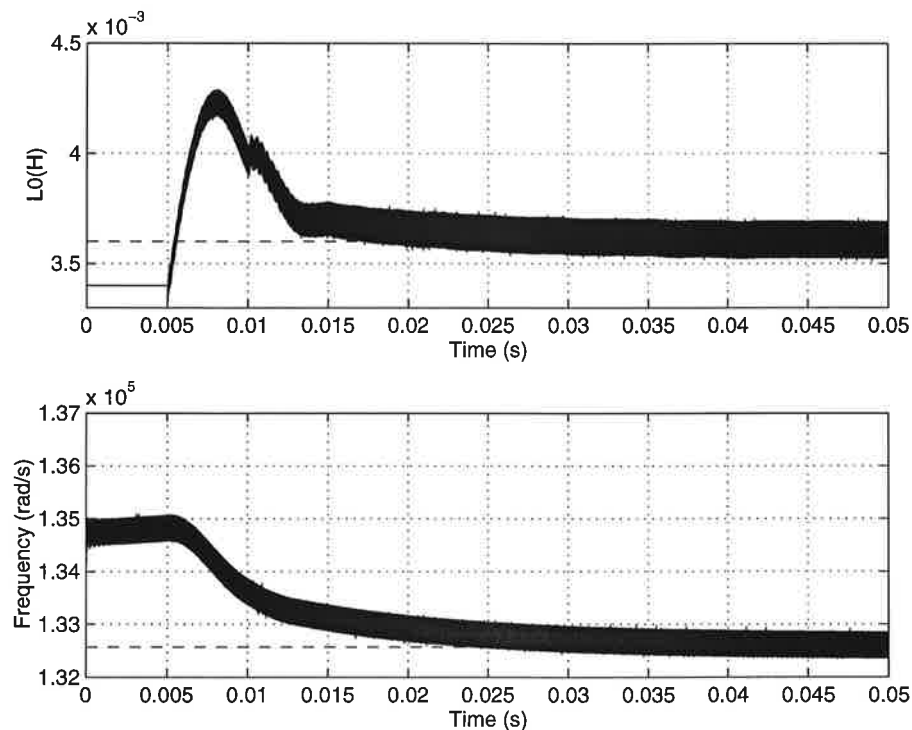


Figure 32. Simulations of L_0 and ω (solid lines) with the *complete* model and desired L_0 and ω (dashed lines). Initial values used: $L_0 = 3.4 \cdot 10^{-3}$ H and $\omega = 134484$ rad/s, i.e. 6% error in L_0 and 300 Hz error in ω . Parameter values used: $R = 70 \Omega$, $C_0 = 15.8$ nF, $C = 2.18$ nF, $L = 2.97$ mH, $\gamma_1 = 0.01$, $\gamma_2 = 0.8$, $K_0 = 10000$, $\tau_1 = 0.001$, $\tau_2 = 10^{-5}$ and $a = 1/0.0007$.

9. Simulations

In previous sections theory for the ultrasonic system has been presented. Some statements about its asymptotic behavior has also been stated. It is of great importance to verify these statements by simulations on a computer. The simulations can also be done without the limiting assumptions made for the mathematical analysis. If the simulated results are consistent with the analytical results, this would validate the approximations and simplifications previously made.

The simulations were made in OmSim, an object oriented simulation program for simulation of dynamical systems.

Simulation of the PLL/Amplitude Setup with L_0 Adjustment

When the ultrasonic system is simulated, the state space description (6) is used. This model, which will be referred to as the *complete model*, has two advantages. First it is simple to implement in OmSim, and secondly it contains states for both the generator current $x_3(t)$ and the amplitude of the converter $x_1(t)$. These states can easily be used for feedback.

In order to verify the theoretical results derived in Section 8, simulation of the system in Figure 23 is made. The generator is simulated with a ramped sinusoidal output signal. It takes 10 ms for the amplitude of the generator voltage to reach its maximum value. Phase detectors are simulated with analog

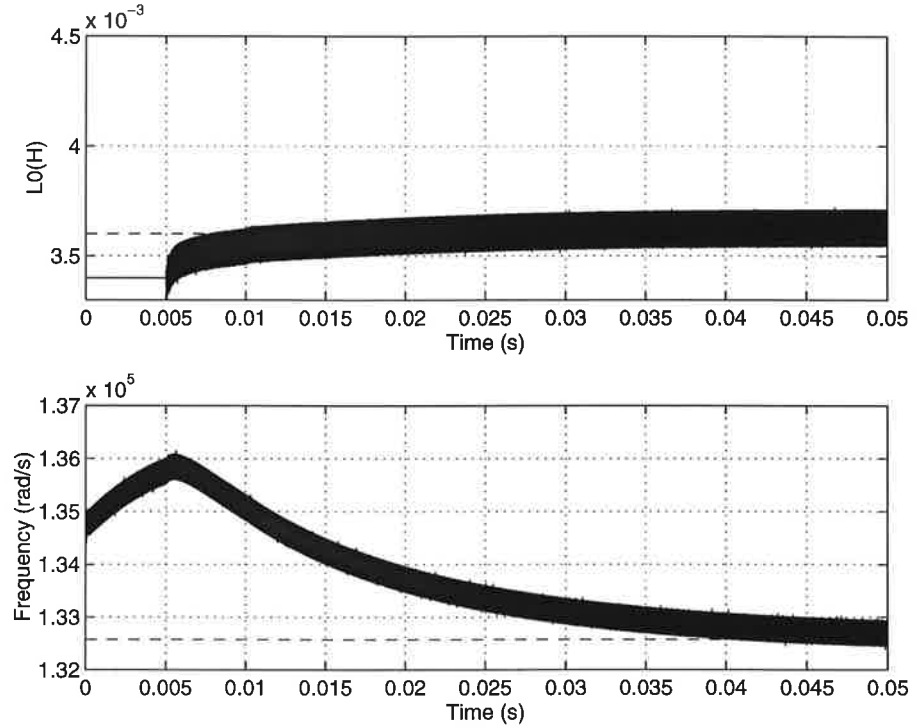


Figure 33. Simulations of L_0 and ω (solid lines) with the *complete* model and desired L_0 and ω (dashed lines). Initial values used: $L_0 = 3.4 \cdot 10^{-3}$ H and $\omega = 134484$ rad/s, i.e. 6% error in L_0 and 300 Hz error in ω . Parameter values used: $R = 700 \Omega$, $C_0 = 15.8$ nF, $C = 2.18$ nF, $L = 2.97$ mH, $\gamma_1 = 0.01$, $\gamma_2 = 0.8$, $K_0 = 10000$, $\tau_1 = 0.001$, $\tau_2 = 10^{-5}$ and $a = 1/0.0007$.

multipliers (PD type 1) acting on square wave signals, followed by either an active or a passive low pass filter. These filters are given by (17) or (18), and the PLL is simulated with an active loop filter. The adjustment of L_0 is made with the second update law, given by (26), and the adjustment is delayed 5 ms to avoid that transients affects the L_0 adjustment.

In Figure 32 simulations of the complete model with amplitude feedback and adjustment of L_0 is shown for $R = 70 \Omega$. Figure 33 shows a simulation of the same system, but this time $R = 700 \Omega$. It is seen that the system reaches its equilibrium point (22). The reason for the thick lines in the figure, is that the signals contains high frequencies. These frequencies are introduced by the phase detectors, and makes the simulations very time consuming. It is possible to reduce the influence of these high frequencies by introducing higher order low pass filters after the phase detectors. Worth noticing is that there is a transient in the L_0 signal in Figure 32 at $t = 10$ ms. This transient is due to the end of the ramping of the generator voltage. No transient is however seen in Figure 33 because that is a simulation of a system with better damping ($R = 700 \Omega$).

The OmSim-code used for this simulation is found in Appendix A, Listing 2.

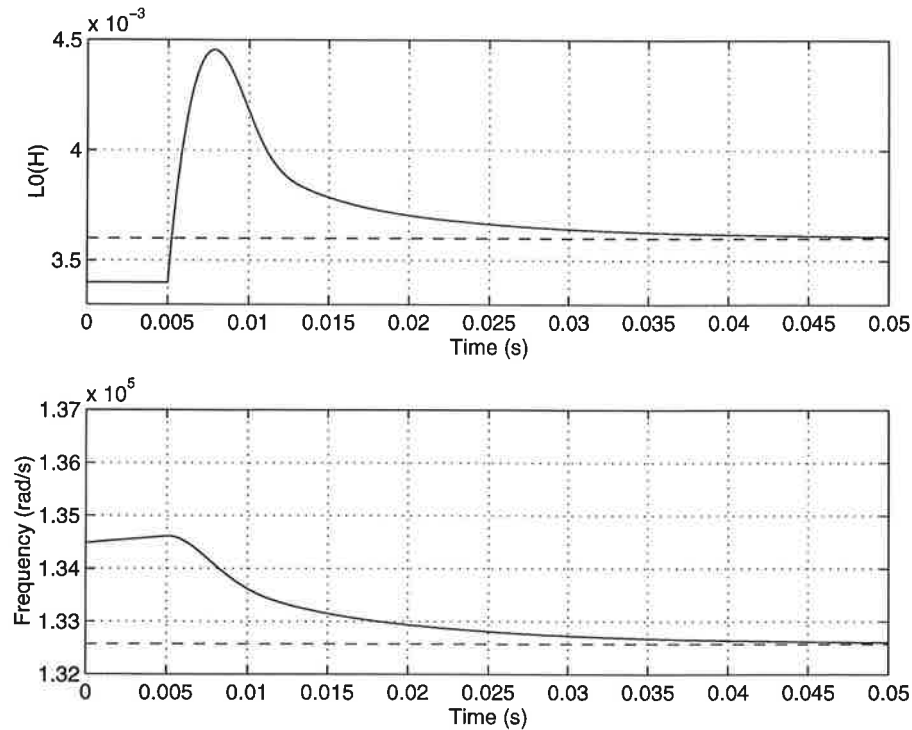


Figure 34. Simulations of L_0 and ω (solid lines) with the *simplified* model and desired L_0 and ω (dashed lines). Initial values used: $L_0 = 3.4 \cdot 10^{-3}$ H and $\omega = 134484$ rad/s, i.e. 6% error in L_0 and 300 Hz error in ω . Parameter values used: $R = 70 \Omega$, $C_0 = 15.8$ nF, $C = 2.18$ nF, $L = 2.97$ mH, $\gamma_1 = 0.01$, $\gamma_2 = 0.8$, $K_0 = 10000$, $\tau_1 = 0.001$, $\tau_2 = 10^{-5}$ and $a = 1/0.0007$.

Simulation of the Simplified System

Simulation of the complete system is very time consuming, due to the high frequencies acting in the system. It would therefore be preferable to use the *simplified model* derived in Section 6, which would speed up the simulations considerably. It is however important to be aware of that this is only an approximation of the real system, and it has to be verified that the simplified model gives reasonable results. This is done in Figure 34 ($R = 70 \Omega$) and Figure 35 ($R = 700 \Omega$) where the same simulation is made of the simplified model (Figure 24) that was made with the complete model previously. The simulation shows that the main characteristics of the complete system is captured by the simplified model (compare Figure 32-33). This motivates the approximation introduced in Section 6 and it justifies the use of this approximation in Section 7 and Section 8.

The OmSim-code used for this simulation is found in Appendix A, Listing 1.

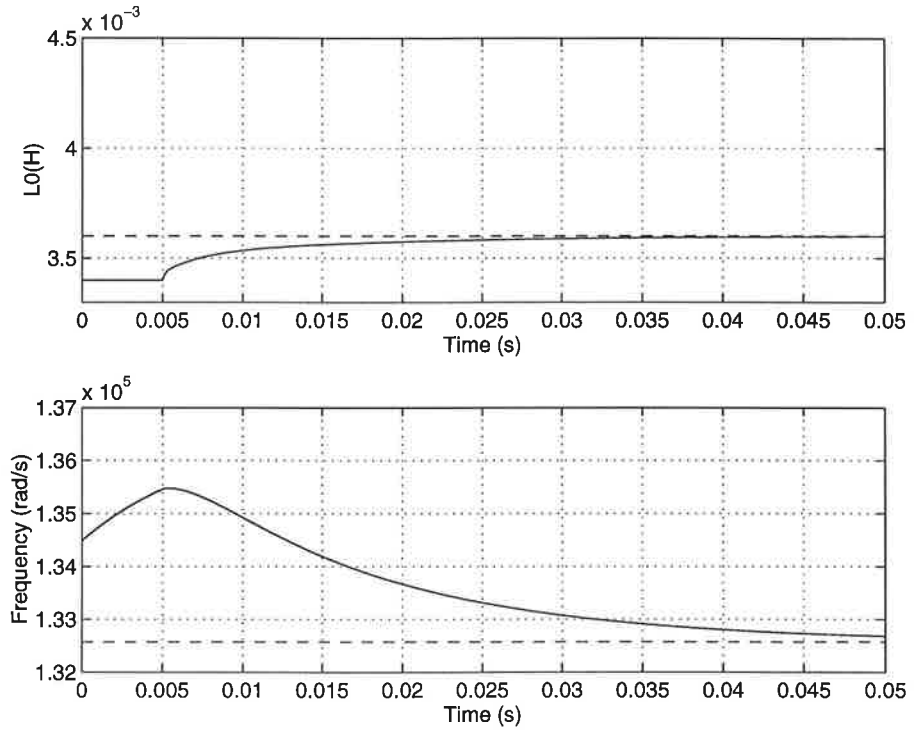


Figure 35. Simulations of L_0 and ω (solid lines) with the *simplified* model and desired L_0 and ω (dashed lines). Initial values used: $L_0 = 3.4 \cdot 10^{-3}$ H and $\omega = 134484$ rad/s, i.e. 6% error in L_0 and 300 Hz error in ω . Parameter values used: $R = 700 \Omega$, $C_0 = 15.8$ nF, $C = 2.18$ nF, $L = 2.97$ mH, $\gamma_1 = 0.01$, $\gamma_2 = 0.8$, $K_0 = 10000$, $\tau_1 = 0.001$, $\tau_2 = 10^{-5}$ and $a = 1/0.0007$.

Summary

In this section the theoretical results derived previously in this thesis have been verified by simulations on a computer. The simulations shows that the simplification introduced in Section 6 is valid, both for small and for high R . It was also shown that the theoretical results derived in Section 8 were valid, i.e. the simulation of the setup with amplitude feedback via a PLL and adjustment of L_0 was succesfull.

10. Concluding Discussion

In this thesis much theory has been presented and a concluding discussion is needed.

Summary

Section 2 dealt with the derivation of two different mathematical models of the ultrasonic sealing unit. The first one, called the admittance model, described the relationship between the voltage and the current of the generator. This is a previously well known model. The second model described the relationship between the voltage of the generator and the amplitude of the converter.

The amplitude model was not previously known, and measurements had to be made to validate the model. This was done in Section 3, and the results showed that the model described the ultrasonic system well.

Once a model of the ultrasonic system was derived, this model could be used to find a solution to the frequency control problem. In Section 4 a recursive least square estimator was used to estimate the resonance frequency of the ultrasonic system. For simplicity only a second order system was considered. A number of possible problems with the RLS approach were presented.

Next an examination of the existing equipment was made, and presented in Section 7. This solution included a phase-locked loop, and the theory for the PLL was presented in Section 5. In order to be able to analyze the PLL, it was transformed into the phase signal domain. When the transformed PLL should be connected to the ultrasonic system, the ultrasonic system also had to be transformed into the phase signal domain. This could be done by an approximation introduced in Section 6, which said that the transients in the phase signal domain could be neglected. With this approximation it was possible to analyze the existing solution, which consisted of a PLL to keep the phase error between the voltage and the generator small, and it was shown that there were some major problems with this solution.

Therefore a new approach to the frequency control problem was taken in Section 8. Now the amplitude of the converter was used as the feedback signal via a PLL. This new setup removed many of the problems with the existing equipment, but the problem with mismatched generator and stack still existed. This problem was removed by introducing an update law of L_0 which adjusted L_0 in such way that the phase error between the voltage and the current of the generator always remained small, i.e. the generator and stack was always well matched. Both theory and simulations showed that this solution could be expected to work well in practice.

Conclusions

In this thesis two major results have been presented. The first important result is the transformation of a linear time invariant system into the phase signal domain, and the approximation of the dynamics of the system in this domain. This approximation is presented in Section 6 and it makes it possible to simplify the mathematical analysis and the simulations of a PLL connected to a linear time invariant system.

The second, and more important, result is the setup with feedback from the amplitude of the converter combined with adjustment of L_0 . Theory for this setup is presented in Section 8 and verified by simulations in Section 9. The new setup eliminates the known problems with the existing setup, and it would have been very interesting to implement this solution in practice. There was however no time to do this, but this thesis shows that it is realistic to assume that the new solution to the frequency control problem will work well in practice.

References

- [1] Roland E. Best. *Phase-locked Loops*. McGraw-Hill, 1983
- [2] Floyd M. Gardner. *Phaselock Techniques, 2nd Edition*. Wiley Interscience, 1979
- [3] Hewlett-Packard. *HP 3566A/3567A Measurement Reference Hardware Service Manual*. A.02.01, May 1991
- [4] Rolf Johansson. *System Modeling & Identification*. Prentice-Hall, 1993
- [5] Ulf Lindblad. *Transmission Line Model of an Ultrasonic Sealing Unit*. Diploma Work, Lund 1994
- [6] Martin Martell. *An Ultrasonic Measuring Method for Determining the Mechanical Loss Factor for some Packaging Materials*. Diploma Work, Lund 1993
- [7] K.J. Åström & B. Wittenmark. *Computer Controlled Systems, 2nd Edition*, Prentice-Hall, 1990
- [8] K.J. Åström & B. Wittenmark. *Adaptive Control*. Addison-Wesley, 1989

Appendix A. OmSim programs

```

LIBRARY ultrasonic;

olin2 ISA Base::Model WITH

K0  ISA Parameter With default := 10000;   END;   % VCO gain
Kd  ISA Parameter WITH default := 0.6366;  END;   % PD gain
tau1 ISA Parameter WITH default := 0.001;  END;   % Filter constant
tau2 ISA Parameter WITH default := 1e-5;   END;   % Filter constant
tau  ISA Parameter WITH default := 0.0007; END;   % Filter constant

C0  ISA Parameter WITH default := 15.8e-9;  END;   % Process parameters
C   ISA Parameter WITH default := 2.18e-9;  END;
R   ISA Parameter WITH default := 70;       END;
L   ISA Parameter WITH default := 29.7e-3;  END;

t0  ISA Parameter WITH default := 0.005;    END;   % Start time of adapt.
gamma1 ISA Parameter WITH default := 0.01;  END;   % Adjustment gain
gamma2 ISA Parameter WITH default := 0.8;    END;   % Adjustment gain

N, fiI, z, L0, L00, t TYPE REAL;           % Variables for the L0-adjustment
w, w0, fiA, z1, z2 TYPE REAL;             % Variables for the PLL

w0 := sqrt((C0+C)/C/C0/L);                % Resonant frequency
t   := Base::Time;

% ===== L0 adjustment =====

N := (R/L*w)^2+(w0^2-w^2)^2;
fiI := -atan(L/R/w*(w0^2-w^2)+C0^2*L^2/R*N*(w*L0-1/w/C0));

z' = 1/tau*(-z + fiI);                    % Passive PD filter

L0' = if t < t0 then 0 else gamma1*z'+gamma2*z; % Update L0

L00 := C*L/(C0+C);                        % Wanted value of L0

% ===== Phase-locked loop section =====

fiA = -atan(R/L*w*(1/L0/C0-w^2)/(w^4-(1/L/C+(L0+L)/C0/L/L0)
          *w^2+1/C0/C/L0/L));

z2' = 1/tau1*fiA;                          % Active loop filter for the PLL
z1 = z2 + tau2/tau1*fiA;

w = Kd*K0*z1+w0;                            % Frequency output from the VCO
END;

```

Listing 1. Simplified model implemented in OmSim.

LIBRARY ultrasonic;

PLL1state ISA Base::Model WITH

```
U0  ISA Parameter WITH default := 1500;  END;  % Voltage amplitude
K0  ISA Parameter WITH default := 10000;  END;  % VCO gain
tau1 ISA Parameter WITH default := 0.001;  END;  % Filter constant
tau2 ISA Parameter WITH default := 1e-5;  END;  % Filter constant
tau  ISA Parameter WITH default := 0.0007;  END;  % Filter constant

C0  ISA Parameter WITH default := 15.8e-9;  END;  % Process parameters
C   ISA Parameter WITH default := 2.18e-9;  END;
R   ISA Parameter WITH default := 70;      END;
L   ISA Parameter WITH default := 29.7e-3;  END;

t0  ISA Parameter WITH default := 0.005;  END;  % Start time of adapt.
t1  ISA Parameter WITH default := 0.010;  END;  % Ramp time

g1  ISA Parameter WITH default := 0.01;   END;  % Adjustment gain 1
g2  ISA Parameter WITH default := 0.8;    END;  % Adjustment gain 2

x1, x2, x3, x4, i, u, w0, uref, te, L0 TYPE REAL;
z1, z2, t, th TYPE REAL;
isign, usign, w TYPE REAL;
i1, PD, PD2, L00, thetai TYPE REAL;

% ===== L0 adjustment =====

PD2 := sign(i1)*usign;          % PD between the current and voltage.

thetae' = 1/tau*(-thetae + PD2);  % Passive PD filter

L0' = if Base::Time < t0 then 0 else g1*thetae'+g2*thetae; % Update L0

L00 := C*L/(C0+C);            % Wanted value of L0

% ===== Phase-locked loop section =====

isign := sign(i);              % Take the sign of the input ..
usign := sign(y1);             % .. signals to get an amplitude ..
% .. independent PD gain.

PD := isign*usign;             % Phase detector in the PLL

z2' = 1/tau1*PD;               % Active loop filter for the PLL
z1 := z2 + tau2/tau1*PD;

te := z1*3.1415/2;             % Calculate the phase error from the PLL

th' = K0*te;                    % Integrator in the PLL

y1 := cos(w0*t + th);
y2 := sin(w0*t + th);
```

```

% State space description of the 4:th order admittance model.

x1' =          x2;
x2' = -1/L/C*x1  -R/L*x2          +1/L*x4;
x3' =          -1/L0*x4 + 1/L0*u;
x4' =          -1/C0*x2 + 1/C0*x3;

i := -x1;          % Electrical analogy for the amplitude
i1 := x3;         % Feedback to the phase detector for L0 adjustment

t := Base::Time;

u := IF t < t1 then t/t1*U0*y2 ELSE U0*y2;    % Output voltage ..
                                           % .. from the generator.

END;

```

Listing 2. Complete model implemented in OmSim.

